Contract No:

This document was prepared in conjunction with work accomplished under Contract No. DE-AC09-08SR22470 with the U.S. Department of Energy (DOE) Office of Environmental Management (EM).

Disclaimer:

Nitric-Glycolic Flowsheet REDuction/OXidation (REDOX) Model for the Defense Waste Processing Facility (DWPF)

C.M. Jantzen
M.S. Williams
T.B. Edwards
C.L. Trivelpiece
W.G. Ramsey
June 2017

SRNL-STI-2017-00005, Revision 0

DISCLAIMER

Printed in the United States of America

Prepared for
U.S. Department of Energy

SRNL-STI-2017-00005
Revision 0

Keywords: *Glycol, Alternate Reductant DWPF, Reduction/Oxidation, REDOX*

Retention: *Permanent*

Nitric-Glycolic Flowsheet REDuction/OXidation (REDOX) Model for the Defense Waste Processing Facility (DWPF)

C.M. Jantzen
M.S. Williams
T.B. Edwards
C.L. Trivelpiece
W.G. Ramsey

June 2017

Prepared for the U.S. Department of Energy under contract number DE-AC09-08SR22470.

Savannah River National Laboratory™
OPERATED BY SAVANNAH RIVER NUCLEAR SOLUTIONS

REVIEWS AND APPROVALS

AUTHORS:

C.M. Jantzen, Waste Form Processing Technologies Date

M.S. Williams, Process Technology Programs Date

T.B. Edwards, Immobilization Technology Date

C.L. Trivelpiece, Immobilization Technology Date

W.G. Ramsey, Chemical Processing Techonologies Date

TECHNICAL REVIEW:

C.J. Martino, Process Technology Programs Date

T.B. Edwards, Immobilization Technology, Reviewed per E7 2.60 Date

C.L. Trivelpiece, Immobilization Technology, Reviewed per E7 2.60 Date

APPROVAL:

F.M. Pennebaker, Manager Date
Chemical Processing Technologies

D. E. Dooley, Manager Date
Chemical Processing Technologies

E. J. Freed, Manager Date
Defense Waste Processing and Saltstone Facility Engineering

ACKNOWLEDGEMENTS

The authors would like to thank Madison E. Caldwell of SRNL Engineering Process Development of the Savannah River National Laboratory (SRNL) who performed the various REDOX procedures and Holly Hall for the timely reallocation of equipment resources. Special thanks are due to Whitney Riley and Kimberly Wyszynski of SRNL's Process Science Analytical Laboratory (PSAL) for $Fe^{2+}/\Sigma Fe$, glycolate, formate, oxalate, nitrate, nitrite, and weight percent solids measurements. The authors are also thankful for the support of Tom White of Analytical Development Directorate (ADD) for development of the caustic quench glycolate analytic measurement method.

This paper was prepared in connection with work done under Contract Nos. DE-AC09-76SR00001, DE-AC09-96SR18500, DE-AC09-08SR22470 with the U.S. Department of Energy.

EXECUTIVE SUMMARY

Control of the REDuction/OXidation (REDOX) state of glasses containing high concentrations of transition metals, such as High Level Waste (HLW) glasses, is critical in order to eliminate processing difficulties caused by overly reduced or overly oxidized melts. Operation of a HLW melter at $Fe^{+2}/\Sigma Fe$ ratios of between 0.09 and 0.33, retains radionuclides in the melt and thus the final glass. Specifically, long-lived radioactive ^{99}Tc species are less volatile in the reduced Tc^{4+} state as TcO_2 than as $NaTcO_4$ or Tc_2O_7, and ruthenium radionuclides in the reduced Ru^{4+} state are insoluble RuO_2 in the melt which are not as volatile as $NaRuO_4$ where the Ru is in the +7 oxidation state. Similarly, hazardous volatile Cr^{6+} occurs in oxidized melt pools as Na_2CrO_4 or $Na_2Cr_2O_7$, while the Cr^{+3} state is less volatile and remains in the melt as $NaCrO_2$ or precipitates as chrome rich spinels. The melter REDOX control balances the oxidants and reductants from the feed and from processing additives such as antifoam.

An electron equivalents (EE) exchange REDOX model was developed at SRNL to balance reductants (e.g., oxalate, coal, sugar, formate, antifoam) and oxidants (e.g., nitrates, nitrites, and manganic species) for any melter feed processed in the Defense Waste Processing Facility (DWPF). The model is represented by the number of electrons gained during reduction or lost during oxidation of various species. The overall relationship between the REDOX ratio of the final glass and the melter feed chemistry is given in terms of the transfer of molar EEs. Argon (Ar) bubbling, that was added to improve melt rate during radioactive melting operations, sparges free oxygen from the melt. The Ar effect and the antifoam impact on the REDOX ratio were quantified in the 2012 DWPF EE REDOX model.

Currently, the DWPF is running a nitric acid-formic acid (NF) flowsheet where formic acid is the main reductant and nitric acid is the main oxidant. During decomposition, formate and formic acid release H_2 and CO gas which requires close control of the melter vapor space flammability. A change to a nitric acid-glycolic acid (NG) flowsheet is desired as the glycolates and glycolic acid release less H_2 gas upon decomposition. This would greatly simplify DWPF processing.

Development of an EE term for glycolate in the NG flowsheet is documented in this study. An interim REDOX model using the theoretical EE term for glycolate was developed in March 2016. Over the past year, additional crucible data were collected during the feed-to-glass conversion to validate the interim model.

Prior to this study, simulated feeds prepared for sludge batch (SB) 6 or SB6, when coupled with a refractory frit like Frit 418, were found to give irreproducible $Fe^{+2}/\Sigma Fe$ ratio determinations using a hot insertion sealed closed crucible (CC) methodology for REDOX known as CC_{hot}. This had been observed during SB4 REDOX testing with Frit 418: the viscosity of the glass in the CC_{hot} test was too high to promote convective mixing in the crucible, producing an inhomogeneous glass. Inhomogeneous glass gives non-uniform $Fe^{+2}/\Sigma Fe$ measurement results. To ensure that the glass viscosity variable was controlled the SRNL REDOX procedure was adjusted to require that the sludge-frit mixture being tested in CC_{hot} have a calculated viscosity of <60 poise at 1150°C. This was the viscosity found to provide a homogeneous glass during SB4 testing. If the sludge-frit mixture, equivalent to a Slurry Mix Evaporator (SME) melter feed, is calculated to have a viscosity of >60 poise, $LiBO_2$ is now required to be added as a flux; lithium metaborate does not impact the overall REDOX of the mixture. While the DWPF melter can process SME feeds up to 110 poise, there is not enough convection in a small crucible to produce a homogeneous glass for REDOX measurement unless the viscosity is <60 poise.

The interim model recommended that the DWPF use the 2012 REDOX model slope and intercept with a glycol EE of 6 and Mn EE=0, respectively, for the NG flowsheet at 100-125% acid stoichiometry as indicated below:

$$\xi_{\text{A-gly}} = \left[\left(2[F] + 4[C] + 4[\text{O}_\text{T}] + 3.39 * eff\,[C_A] + 6[Gly] - 5[N] - 0[Mn] \right) \frac{45}{T} \right]$$

where [F] = formate (mol/kg feed)
[C] = coal (carbon) (mol/kg feed)
$[\text{O}_\text{T}]$ = $\text{oxalate}_{\text{Total}}$ (soluble and insoluble) (mol/kg feed)
$[\text{C}_\text{A}]$ = carbon from antifoam (mol/kg feed)
eff = effective antifoam impact = 0.85
[Gly] = glycolate (mol/kg feed)
[N] = nitrate + nitrite (mol/kg feed)
[Mn] = manganese (mol/kg feed)
T = total solids (wt%)
$\xi_{\text{A-gly}}$ = EE term with antifoam and glycolate

and

$$\frac{Fe^{2+}}{\Sigma Fe} = 0.2358 + 0.1999\xi_{A-gly}$$

where Fe^{2+} is the amount of reduced iron in sample divided by the total iron in the sample expressed as the sum of the Fe.

An EE of 6 for glycolate is the theoretical number of electrons transferred when a mole of glycol in the feed converts to CO_2 in the off-gas in the DWPF melter. A de minimis value of 800 mg/kg of antifoam, which is equivalent to 0.03267 mol/kg of carbon from antifoam in the feed. This near zero mol/kg of carbon only imparts a 0.01 difference in the calculated REDOX using the equation above. Acid stoichiometries of 76.9 to 123.2% (Koopman minimum acid, KMA, basis or 80-129% on the Hsu minimum acid basis) were examined in this study. In this range the Mn EE=0 term is valid. The Mn EE=0 term may be valid at lower glycolic acid stoichiometries but potentially high nitric concentrations with low glycolic acid concentrations could cause the manganese term to oxidize to greater than +2.

The data shown in the current study validated the interim REDOX model given above with a glycolate EE of 6 and Mn = 0 for the NG flowsheet. The weight percent (wt%) solids term, 45/T, was shown to be deviate from linearity for values less than 32% total solids. The further below 32% total solids, the larger the deviation from linearity. Since 32% total solids, which includes the frit contribution, is close to the DWPF insoluble solids and yield stress design bases, it is recommended that a DWPF facility limit be imposed during implementation of the NG REDOX model. The NG REDOX model is more sensitive to the 45/T compositional concentration adjustment term because glycolate has a large EE of 6 compared to the NF REDOX model under which DWPF has operated, i.e. the main reductant (formate) only had an EE of 2..

Because the final NG REDOX model is based on the same balance between the oxidizers and reductants in the melter as previous NF REDOX models, then the pilot-scale and full-scale DWPF validation data from the NF flowsheet apply as scale-up validation. However, it is recommended that glass pour spout samples be taken during the transition from the NF to the NG flowsheet and several after steady state with the NG flowsheet has been achieved.

This study demonstrates the following:

- the final NG REDOX model and the interim NG REDOX model are the same
- the final NG REDOX model cannot be used on feeds less than 32wt% SME solids unless a mathematical algorithm is developed for feeds with <32wt% SME solids
- the final NG REDOX model has an Mn EE term of zero in the range of acid stoichiometries examined in this study (76.9 to 123.2% KMA basis or 80-129% on Hsu basis): lower concentrations of glycolic acid in the presence of higher nitric acid would need to be investigated to determine if the Mn EE=0 is still valid

This study recommends the following:

- Since 32% total solids, which includes the frit contribution, is close to the DWPF insoluble solids and yield stress design bases, it is recommended that a DWPF facility limit be imposed during implementation of the NG REDOX model.
- pour spout (PS) samples be taken to confirm the NG REDOX model as was done with the NF REDOX model
- the linearity of the Ar term during processing with the NG flowsheet be checked with data from the PS samples

TABLE OF CONTENTS

LIST OF TABLES

LIST OF FIGURES

LIST OF ABBREVIATIONS

ADD	Analytic Development Directorate
ANOVA	Analysis of Variance
BP	Blended Product
CC	Closed (sealed) crucible
CC_{Ar}	Closed (sealed) crucible with Ar bubbling
CC_{hot}	Closed (sealed) Crucible with hot insertion
CC_{ramp}	Closed (sealed) Crucible with temperature ramp
CCOG	Closed (sealed) Crucible with off-gas measurement
CEF	Cold-cap Evaluation Furnace
CWAO	Catalytic Wet Air Oxidation
DSC	Differential Scanning Calorimetry
DWPF	Defense Waste Processing Facility
EE	Electron Equivalents
ELN	Electronic Laboratory Notebook
H&S	Heat & Stop Experiments
HLW	High Level Waste
HSD	Honestly Significant Difference
HTXRD	High Temperature X-Ray Diffraction
IDMS	Integrated DWPF Melter System
KMA	Koopman Minimum Acid
LHS	Left Hand Side
MFT	Melter Feed Tank
MM	Mini-Melter
MRF	Melt Rate Furnace
MTS	Methyl Tri Siloxane
NF	Nitric-Formic
NG	Nitric-Glycolic
OLS	Ordinary Least Squares
PEO	Poly Ethylene Oxide
PRA	Percent Reducing Acid
PS	Pour Spout
PSAL	Process Science Analytical Laboratory
REDOX	REDuction/OXidation
RHS	Right Hand Side
RMSE	Root Mean Square Error
SB	Sludge Batch
SEM	Scanning Electron Microscope
SGM	Scale Glass Melter
SME	Slurry Mix Evaporator
SMRF	Slurry-Fed Melt Rate Furnace
SRAT	Sludge Receipt and Adjustment Tank

SRNL	Savannah River National Laboratory
SRS	Savannah River Site
SRTC	Savannah River Technology Center
T	Total Solids
TOC	Total Organic Carbon
WTP	Waste Treatment Plant
WVDP	West Valley Demonstration Project
XRD	X-ray Diffraction

1.0 Introduction

Savannah River Site (SRS) High Level Waste (HLW) sludge is immobilized by vitrification into borosilicate glass at the Defense Waste Processing Facility (DWPF). During production of HLW glass, the REDuction/OXidation (REDOX) of the melt pool cannot be measured.[f] Therefore, the $Fe^{2+}/\Sigma Fe$ REDOX ratio in the glass poured from the melter has been related to melter feed organic and oxidant concentrations to ensure production of a high quality glass without impacting production rate (e.g., foaming) or melter life (e.g., metal and/or metal sulfide formation and accumulation on the melter bottom).

The DWPF REDOX model is used to control the ratio of melter feed reductants and oxidants between a $0.09< Fe^{2+}/\Sigma Fe <0.33$ production range. Controlling HLW melter at a REDOX equilibrium of $Fe^{2+}/\Sigma Fe \leq 0.33$ [1, 2] prevents the formation of undesired metallic or metal sulfide deposits on the bottom of the melter during vitrification. The lower REDOX limit eliminates melter foaming from deoxygenation of manganic oxides. Above the lower REDOX limit of $Fe^{2+}/\Sigma Fe \geq 0.09$ about 99% of the manganic species are converted to Mn^{2+} [1, 2] and oxygen is not released during melting.

In summary, the REDOX equilibrium in Joule-heated HLW melters is controlled to prevent the following:

- The potential for (1) metallic species such as $NiO \rightarrow Ni° + ½\ O_2$ and $RuO_2 \rightarrow Ru° + O_2$ or sulfate ($SO_4^{=}$) or (2) sulfide ($S^{=}$) species to couple with species such as Ni^{2+}, Ni°, Cu^{2+}, or Cu° forming Ni_2S_3 and Cu_2S metal sulfides and/or Ni°-Cu° alloys (Figure 1-1)
- The potential for the metallic species and/or sulfides to fall to the melter bottom and cause shorting of electrical pathways in the melt and accumulations which may hinder glass pouring.
- The potential for overly reduced glasses, which can be less durable than oxidized equivalents [3].
- The potential for elevated corrosion rates of the reduced K-3 refractory used to line HLW melters at SRS, West Valley Demonstration Project (WVDP), and Waste Treatment Plant (WTP) in Hanford [4, 5].

The target REDOX for the world's largest operating HLW melter, the SRS DWPF melter, has been an $Fe^{2+}/\Sigma Fe$ ratio of 0.2 which is in the middle of the $0.09> Fe^{2+}/\Sigma Fe <0.33$ production range. This ratio minimizes release of radionuclides (such as ^{99}Tc and ^{104}Ru) and hazardous species (such as Cr^{6+}).

Recently, the DWPF implemented bubbling to increase the melt rate of the incoming feeds and improve melt pool convection [6]. The DWPF made a decision not to bubble air as this would create an oxidized melt pool but to bubble argon (Ar) gas instead due to the advantages discussed above for volatilization of ^{99}Tc, ^{104}Ru, and Cr^{6+}. Argon sparges or degasses excess oxygen from the melt and creates a more reduced melt [7, 8, 9]. Therefore, the Ar impact was quantified so that the overall REDOX, including the impact of Ar, could continue to be targeted at $Fe^{2+}/\Sigma Fe=0.2$ in the middle of the $0.09> Fe^{2+}/\Sigma Fe <0.33$ production range.

1.1 The Role of Reductants and Oxidants in Defense Waste Processing Facility (DWPF) Processing

The REDOX model is used to control the balance of feed reductants and oxidants in the pre-melt processing tank known as the Sludge Receipt and Adjustment Tank (SRAT). While some oxidants and reductants are present in the waste additional oxidants and reductants, such as formic acid and nitric acid,

[f] Attempts are currently being made to use REDOX probes but this has yet to be proven to work in an operating radioactive facility.

are added to facilitate processing. These acids are refluxed in the SRAT and analysis of dried SRAT product indicates that alkali/alkaline earth salts such as $NaNO_3$ and NaCOOH, are formed [10, 11, 12]. The chemical balance of oxidants and reductants that is set by the end of the SRAT cycle can only be altered by the addition of oxidants or reductants to the Slurry Mix Evaporator (SME). The melter REDOX balance imposed by the reductants and oxidants can be altered by sparging with an oxidizing (air) or inert (Ar) gas; air can make the melt pool more oxidizing and Ar sparging can make the melt pool more reducing.

In the SRAT, oxidizing and reducing acids are added to the waste sludge [13] for the following reasons:

- control potential melt foaming which adversely impacts melt rate by:
  - destroying nitrites
  - converting carbonates in the feed to CO_2 which vaporizes in the SRAT off-gas rather than in the melter and
  - converting a large fraction [14] of the oxidized Mn^{4+} or Mn^{3+} present as MnO_2, Mn_2O_3, Mn_3O_4, or $NaMn^{7+}O_4$ and/or hydrous complexes in the feed to $Mn^{2+}O$ or $Mn^{2+}(COOH)_2$, so that oxygen from the +4 to +2 conversion is liberated in the SRAT to the solution rather than liberated as O_2 gas in the melter;
- reduce and steam strip mercury for subsequent removal, $HgO \rightarrow Hg°$; and
- improve slurry rheology by neutralizing excess hydroxide (OH^-) in the feed

The SRAT product is then fed to the SME, where borosilicate glass frit slurry is added to produce the melter feed slurry. The melter feed slurry is nominally concentrated to 30-50 weight percent (wt%) total solids in the SME and then fed to the Melter Feed Tank (MFT). The MFT is a holding tank for transfers into the Joule-heated melter where the feed is vitrified at 1150°C.

The NaCOOH and $NaNO_3$ salts react in the melter cold cap at elevated temperatures: the reaction of these salts in the cold cap controls the melter REDOX.

1.2 DWPF Nitric-Acid Formic Acid (NF) Flowsheet

The first REDOX model developed for DWPF balanced formic acid concentrations expressed as [F] and nitric acid concentrations expressed as [N] with a 1:1 molar stoichiometry [15, 16, 17, 18]. This model implied that the oxidizing power of nitric acid was equivalent to the reducing power of formic acid on a molar basis. During this initial crucible study, it was shown that the relationship between the $Fe^{2+}/\Sigma Fe$ ratio and the {[F]-[N]} summation was "S" shaped (Figure 1-1). All {[F]-[N]}<0.9 were on a REDOX plateau of $Fe^{2+}/\Sigma Fe<0.05$ (the bottom of the "S" shape. For overly reduced glasses and {[F]-[N]}>1.7), the absolute concentrations of formate and nitrate had no appreciable effect on glass REDOX either and a second plateau formed at a $Fe^{2+}/\Sigma Fe$ of ~0.65 (the top of the "S" shape). In this overly reduced regime, excess reductant reduced >60% of the ferric iron to ferrous and then began conversion of $NiO \rightarrow Ni°$ and $1.5SO_4^{=} \rightarrow 1.5S^{2-} + 3O_2$, causing Ni_3S_2 and/or Ni° to form (Figure 1-1). In the range between the two plateaus, the $Fe^{2+}/\Sigma Fe$ response was linear with respect to {[F]-[N]} and a model was fit to the data.

In 1997, the data used to develop the {[F]-[N]} relationship was revisited because inclusion of any data from the two plateau regions can highly leverage the Ordinary Least Squares (OLS) fit to the data. Hence, glass quality and REDOX measurement criteria were developed to screen the data used for modeling. This redefined the population of glasses by excluding those below one half the $Fe^{2+}/\Sigma Fe$ measurement detection limit of 0.03 or 0.015 (the bottom of the "S") and those that precipitated metallic and/or sulfide species (the top of the "S") [19]. Averaging of formate, nitrate and measured REDOX ratios was used to minimize model error. Regression of the redefined data demonstrated that the {[F]-[N]} parameter was a

less accurate predictor (Root Mean Square (R^2)=0.68) of waste glass REDOX than had previously been calculated. The regression of the redefined data [19] showed that there was an {[F]-3[N]} relationship between the feed reductants, oxidants, and the glass REDOX ratio,

Equation 1 $Fe^{2+}/\Sigma Fe = 0.217 + 0.253[F]-0.739[N]$, $R^2=0.89$

where the [F] and [N] are normalized to a feed that is 45 wt% solids as the concentrations of F and N are dependent on the solid and liquid concentrations in the feed.[t] Equation 1 was used during DWPF initial operations (Sludge Batch (SB) 1 and SB2) when off-gas surges were common. The surges were studied by neural net modeling of thirty-nine DWPF melter parameters. This modeling indicated that melter feed flow and melter level (which includes any contributions from foam generation) had a direct impact on the melter pour surges [20] and a more reducing flowsheet was adhered to from SB2 on.

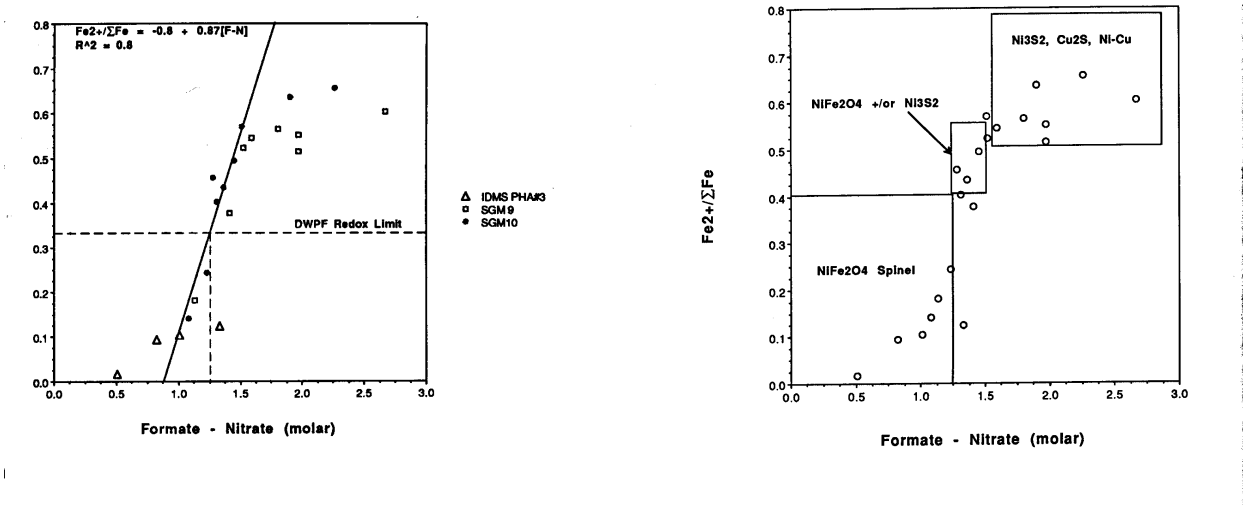

Figure 1-1. Relationship between the Measured REDOX ratio (y axis) and the Difference Between the Feed Reductants (formate) and Oxidants (nitrate).
The "S" Shaped Curvature of the Relationship is Demonstrated Along with the Linear Portion used for Modeling.
SGM is the Slurry Fed Glass Melter and IDMS is the Integrated DWPF Melter System.

Both the {[F]-[N]} and the {[F]-3[N]} REDOX models assumed that the melter feeds were properly formated and refluxed to ensure that 66-100% of the Mn^{3+} and Mn^{4+} were converted to Mn^{2+} as $Mn(COOH)_2$ during preprocessing in the SRAT, e.g., before the melter feed entered the melter. The goal of reducing 66-100% of manganese to avoid oxygen foaming in the melter is based on work performed in the 1980's as summarized by Plodinec in 14, 21. The experiments, which were performed in the absence of nitrates, indicated that melter foaming from oxygen liberation would not be extensive in a HLW melter using formic-acid for reduction if a minimum of 66% of the oxidized Mn^{4+} present in a waste feed were reduced to Mn^{2+} prior to vitrification.
Both the {[F]-[N]} and the {[F]-3[N]} REDOX models demonstrated that the REDOX model balances the reductants and the oxidants so that the slope of an x-y plot of oxidants vs reductants has a slope of ~1 and an intercept of ~0 (Figure 1-2a) for the historic REDOX data (Appendix A) only, i.e. the formic/nitric flowsheet. Figure 1-2a demonstrates that when the oxidants and reductants are balanced exactly, they are

[t] The water content of a melter feed alters the species concentrations of the reductants and oxidants and can influence the equilibrium oxygen fugacity (f_{O_2}) in a melter during vitrification. Since the effects of water on oxygen fugacity are small relative to the impact of dilution on feed concentrations, the molar concentrations were transformed to a 45% solids basis.

on the 1:1 line shown and that the 1:1 line in Figure 1-2a corresponds to the zero line in Figure 1-2b, where the oxidants are subtracted from the reductants and plotted against the measured REDOX. Excess oxidants are below the 1:1 line in Figure 1-2a and to the left of zero in Figure 1-2b. Excess reductants are above the 1:1 line in Figure 1-2a and to the right of zero in Figure 1-2b.

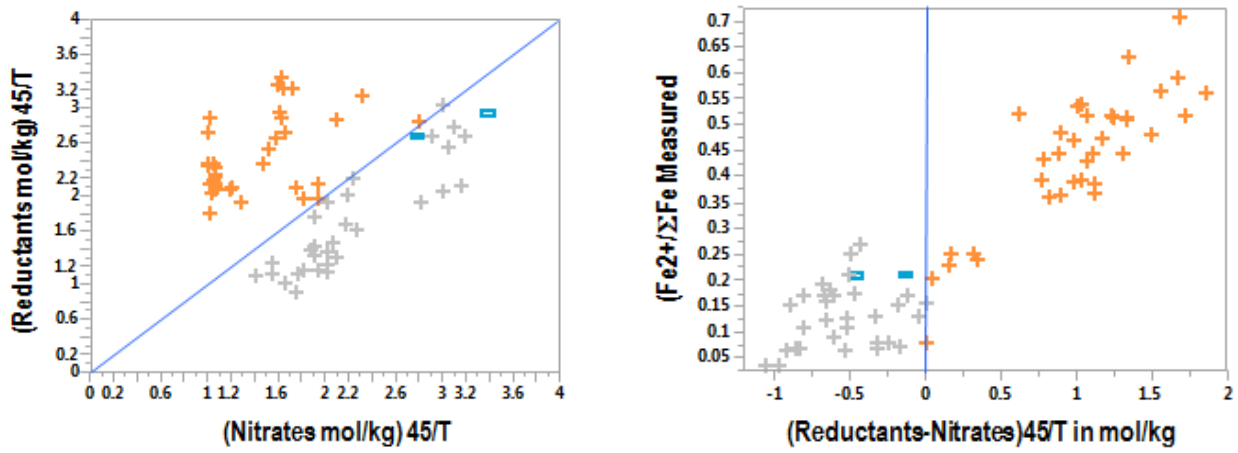

(a) (b)

Figure 1-2. (a) Historic Data Reductants (formic acid only) vs. Oxidizers (nitrates only) weighted by 45/T where T is the weight percent solids. (b) Historic Data Reductants minus Oxidizers.
The DWPF REDOX model is developed by fitting a slope and intercept to the data in figure "b".
The two horizontal rectangles represent SB2 SRAT/SME 224. Gray plus signs are feeds used in crucible tests with excess oxidizers and orange plus signs are feeds with excess reductants.

1.3 The Role of Reductants and Oxidants in the REDuction/OXidation (REDOX) Model

During feed-to-glass conversion, the REDOX reactions occur primarily in the cold cap along with feed decomposition and calcination. In the melt pool, further degassing and homogenization occur primarily by additional REDOX reactions. The gaseous products from the cold cap and the volatile feed components further react with air in the melter vapor space. In order to represent the gradual nature of the feed-to-glass conversion, a 4-stage cold cap model was developed [22], which approximates the melting of feed solids as a continuous, 4-stage counter-current process [23]. In Stage 1 formate salts formed in the SRAT, such as NaCOOH[f], are decomposed to CO, CO_2 and H_2 or steam. The Na forms oxides or otherwise interacts with any silicate, borate, or aluminate species available in the cold cap. The CO subsequently gets oxidized by the air diffusing into the cold cap from the melter plenum and by the oxygen being liberated during the Stage 2 denitration reactions (at further depth in the cold cap). Thus, a generalized set of decomposition and calcination reactions occurring in Stages 1 and 2 can be represented [22, 23] by the combined equation:

Equation 2

$$\underbrace{2NaCOOH + 2NaNO_3}_{melter\ feed\ reductants\ and\ oxidants} \rightarrow \underbrace{CO\uparrow + CO_2\uparrow + H_2\uparrow}_{Stage\ 1} + \underbrace{N_2O\uparrow + 2O_2\uparrow}_{Stage\ 2} + \underbrace{2Na_2O}_{Stage\ 1\ and\ 2} \rightarrow$$

$$\underbrace{2CO_2\uparrow + H_2O\uparrow + N_2\uparrow + 1.5O_2\uparrow}_{plenum} + \underbrace{2Na_2O}_{glass}$$

[f] While the example equations are written as the sodium salts, i.e., NaCOOH, it should be noted that such species as $Ca(COOH)_2$, $Ni(COOH)_2$, $Mn(COOH)_2$ form and undergo similar reaction.

Multiple oxides begin to form during Stage 3. These oxides are assumed to form solid solutions such as spinels which coexist with the REDOX active reductants and oxidants . Stage 4 represents the final fusion where the oxides formed in Stage 3 form aluminate, borate, or silicate groups in the melt, e.g., Fe_2SiO_4 and Na_2SiO_3 (Equation 3).

In order to represent all four stages of cold cap reaction simultaneously (omitting the intermediate CO, N_2O, and NO species produced in Stage 1 and Stage 2 in the cold cap reactions) and include terms for reduced and oxidized iron and silica, one can assume a generalized or equilibrium form of Stages 1-4 cold cap reactions as follows:

Equation 3 $$Fe_2O_3 + 5SiO_2 + 6NaCOOH + 2NaNO_3 \rightarrow Fe_2SiO_4 + 6CO_2\uparrow + N_2\uparrow + 4Na_2SiO_3 + 3H_2O\uparrow$$

Equation 3 assumes that Fe^{3+} enters the melter as Fe_2O_3 and that the reductant $COOH^-$ and the oxidizer NO_3^- enter as sodium formate and sodium nitrate salts, respectively. The formated and nitrated salts react with glass formers (such as SiO_2) to form Fe^{2+} and Na^+ silicate components in the glass and liberate CO_2, N_2, and H_2O vapors to the melter plenum (Equation 3). If oxidants are undersupplied in the melter some CO instead of CO_2 may be present in the off-gas. If reductants are undersupplied in the melter, some NO or N_2O may be present in the off-gas.

For simplicity and consistency in prediction, a mechanistic REDOX model was developed using a *generalized form* of the cold cap reactions (Equation 3). This equation can be rewritten in terms of $2Fe^{2+}$ and $2Fe^{3+}$ instead of the iron oxides and the SiO_2 term can be omitted as it is not involved in the REDOX reactions, e.g., it does not change oxidation state. In addition, the product phases on the right-hand-side (RHS) of the REDOX equilibrium do not consider the intermediate gaseous species generated in Stage 1 and Stage 2 of the cold cap (Equation 3). The left-hand-side (LHS) of the REDOX equilibrium (Equation 3) represents the SRAT/SME reductant and oxidant salts that react in the cold cap.

1.4 DWPF NF Flowsheet with Oxalate, Coal, and Manganese

Sludge Batch 3 was purported to contain high concentrations of reductants that were not in the simple formate vs. nitrate REDOX correlations used for SB1 and SB2: species such as oxalate and coal. After SB2, but before SB3, it was recognized that the 1:3 relationship between formic acid and nitric acid in Equation 1 was related to the number of electrons transferred by the carbon in formate as it was oxidized and in the nitrogen in nitrate as it was reduced.

Thus a REDOX model using Electron Equivalents (EE) transferred during the REDOX reactions was developed with terms for the additional reductants [24, 25] based on the cold cap interactions discussed in the Section 1.3. In addition, a manganese term was added to the EE model to account for potential differences in the oxidation state of Mn in the feed (+4) and in the glass (+2) as it could not be guaranteed that 66-100% of the manganese was reduced to $Mn(COOH)_2$ in the SRAT. When coal and oxalate were absent, the EE model reverted to an {[F]-2.5[N]} stoichiometry plus the term for manganese.

Using the EE approach generates Equation 4 as the controlling REDOX reaction between reducing formate salts and oxidizing nitrated salts, in the melter cold cap:

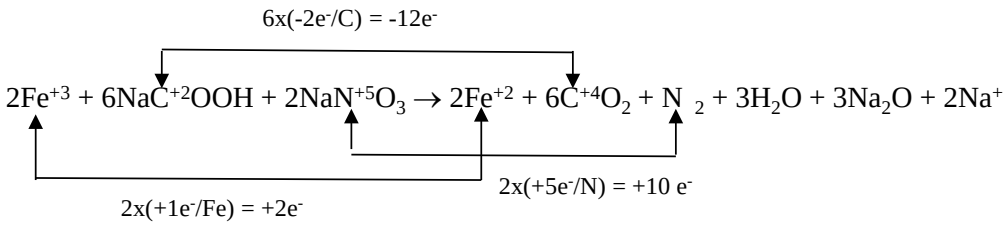

Equation 4

The REDOX equilibrium shown in the Equation 4 between nitrate salts and formate indicates that one mole of nitrate gains 5 electrons when it is reduced to N_2 while one mole of carbon in formate loses 2 electrons during oxidation to CO_2. This is an oxidant:reductant ratio of 5:2 which indicates that nitrate is approximately 2½ times as effective an oxidizing agent as formate is a reducing agent (when nitrogen gas is the reaction product). If the formate exchanges 2 EE per mole of carbon, the nitrate exchanges 5 EE per mole of nitrate.

The REDOX equilibrium shown in Equation 5 between nitrate salts and coal indicates that one mole of nitrate gains 5 electrons when it is reduced to N_2 while one mole of carbon in coal loses 4 electrons during oxidation to CO_2. This is an oxidant:reductant ratio of 5:4 which indicates that nitrate is only 1¼ times as effective an oxidizing agent as coal is a reducing agent (when nitrogen gas is the reaction product). If the coal exchanges 4 EE per mole of carbon, the nitrate exchanges 5 EE per mole of nitrate.

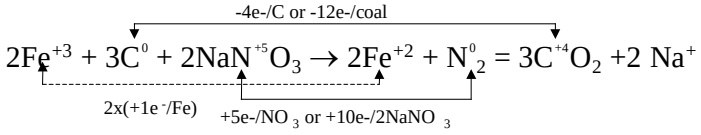

Equation 5

The oxidation/reduction equilibrium between the oxalate and nitrate salts is given in Equation 6.

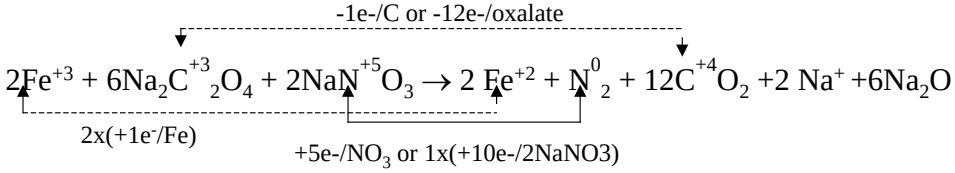

Equation 6

This reaction, written in the format of the preceding cold cap reactions, indicates that one mole of nitrate should gain 5 electrons when it is reduced to N_2 while one mole of carbon in oxalate should lose 1 electron during oxidation to CO_2. This is an oxidant:reductant ratio of 5:2 (since there are 2 moles of carbon in a mole of oxalate). This indicates that nitrate is 2½ times as effective an oxidizing agent as the two carbons in oxalate are a reducing agent (when nitrogen gas is the reaction product).

However, the REDOX modeling data indicated that oxalate was twice as strong a reductant as would be indicated by a 2½:1 ratio. During further investigation of the apparent increase in the reducing power of oxalate, data became available that demonstrated that oxalate salts convert to oxalic acid, which then forms formic acid and CO_2 during SRAT processing [26]. The process was later identified in Reference 27 as spontaneous catalytic wet air oxidation (CWAO) of the oxalate which proceeds with a formate as an intermediate product. If CWAO occurs in the cold cap then six moles of oxalate become 12 moles of formate and 4 EE are exchanged per oxalate overall (Equation 7).

Equation 7

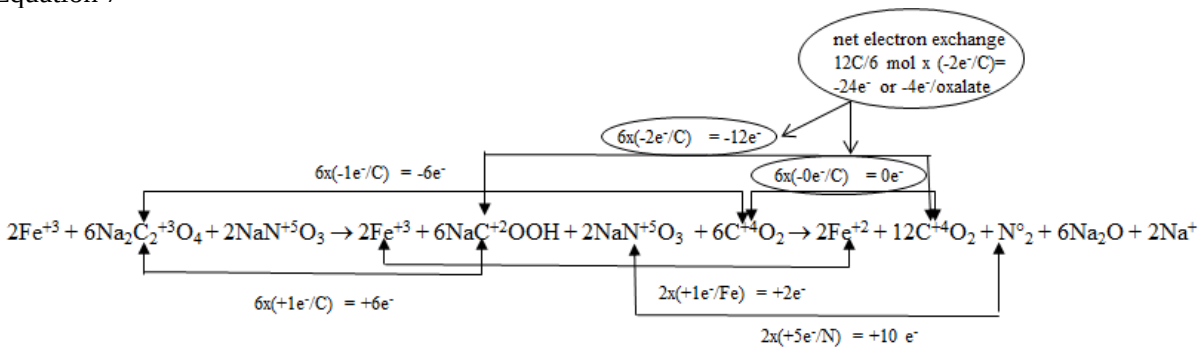

Koopman also identified that spontaneous CWAO is not limited to oxalate but could occur with other reductants such as formate and antifoam [28]. However, during REDOX modeling of formate, antifoam, and other reductants, the experimental data did not indicate that any of these terms were twice as strong a reductant due to CWAO.

An electron transfer equation was written for the reduction of manganese by any carbon containing reductant. The equation assumed that the manganese entered the melter as Mn^{+4} either from the sludge where it can be present as $Mn^{3+}OOH$, Mn_3O_4 (mixed Mn^{4+} and Mn^{2+}), $Mn^{4+}O_2$, jacobsite (Fe_2MnO_4), mixed unidentified Fe-Mn oxides/hydroxides [29] or from SRAT processing. During SB3 SRAT processing, the distribution of the soluble manganese, that is Mn^{2+}, showed no relation to any combination of feed oxidizers or reductants. This is because manganese can complex with formate as soluble $Mn(COOH)_2$ in the SRAT supernate, as insoluble MnO_2 in the SRAT insoluble solids, or as insoluble manganous oxalate ($C_2MnO_4 \bullet 2H_2O$) in the SRAT insoluble solids. The role as $Mn(COOH)_2$ is pH dependent, e.g. $Mn(COOH)_2$ is stable at-near neutral pH while aqueous Mn^{+2} is soluble at lower SRAT pH values. Therefore, a measurement of the soluble Mn in the SRAT supernate is insufficient to determine if 66% of the Mn^{4+} has been reduced to Mn^{2+} when the SRAT/SME pH values fluctuate and oxalate is present.

X-Ray Diffraction (XRD) analysis of the dried SRAT solids also showed the presence of manganous oxalate and ferrous oxalate which is isostructural ($C_2FeO_4 \bullet 2H_2O$) and indistinguishable from manganous oxalate during XRD analysis. Subsequent Scanning Electron Microscopy (SEM) analyses of the dried SRAT product also indicated the presence of $MnSO_4$,. Since the distribution of $Mn^{+2}/Mn^{+3}/Mn^{+4}$ in the SRAT product was inconclusive and the REDOX ratio was found to be highly dependent on the molar concentration of MnO in a glass during SB3 testing [24, 25], a manganese term was included in the EE REDOX model. The manganese was conservatively assumed to be all Mn^{+4} and Equation 8 was used to determine the electron transfers between Mn^{+4} conversion to Mn^{+2} in the cold cap.

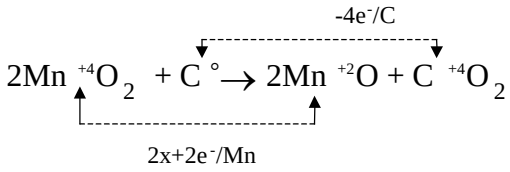

Equation 8

Therefore, the number of electrons gained during reduction or lost during oxidation are the following:

- $[NO_3]$ = +5
- [Mn] = +2
- $[C]_{formate}$ = -2
- $[C]_{coal}$ = -4

- $[C]_{oxalate}$ = -4

The water content of a melter feed alters the species concentrations of the [reductants] and [oxidants] and can influence the equilibrium oxygen fugacity (f_{O_2}) in a melter during vitrification. Since the effects of water on oxygen fugacity are small relative to the impact of dilution on feed concentrations, the molar concentrations were transformed to a 45% solids basis as was done in previous REDOX modeling.

The overall relationship between the REDOX ratio and the EE, ξ, can then be expressed as:

Equation 9
$$\frac{Fe^{2+}}{\Sigma Fe} = f\left[\left(2[F]+4[C]+4[O_T]-5[N]-2[Mn]\right)\frac{45}{T}\right] = f[\xi]$$

where f = indicates a function
[F] = formate (mol/kg feed)
[C] = coal (carbon) (mol/kg feed)
$[O_T]$ = $oxalate_{Total}$ (soluble and insoluble) (mol/kg feed)
[N] = nitrate + nitrite (mol/kg feed)
[Mn] = manganese (mol/kg feed)
T = total solids (wt%)

When the REDOX data generated from SB3 and the historic REDOX data [19] are then fit as a linear function of ξ:

Equation 10
$$\frac{Fe^{2+}}{\Sigma Fe} = 0.1942 + 0.1910\xi$$

The EE REDOX model was generated with an adjusted R^2 of 0.8037 and a Root Mean Square Error (RMSE) of 0.0690 for 120 data observations (53 from the SB study and 67 from the historic study; Appendix A).

During validation of the EE REDOX model [24, 25] against production melter data from WVDP, a melter that used sugar as a reductant, a term for sugar was added to Equation 9. The sugar electron transfers were calculated as:

Equation 11
$$8Fe^{+3} + \overset{0}{C}_{12}H_{22}O_{11} + 8Na\overset{+5}{N}O_3 \rightarrow 8Fe^{+2} + 4\overset{0}{N}_2 + 12\overset{+4}{C}O_2 + 11H_2O + 8Na^+$$
(sucrose)
–4e⁻/C or –48 e⁻/sucrose
8x(+1e⁻/Fe)
4x(+10e⁻/2NaNO₃)

When a term is added for the reductant sugar, the EE term in Equation 9 becomes

Equation 12
$$\xi = \left[\left(2[F]+4[C]+4[S]+4[O_T]-5[N]-2[Mn]\right)\frac{45}{T}\right]$$

where [S] = sugar carbon (mol/kg feed).

1.5 DWPF NF Flowsheet with Oxalate, Coal and Higher Manganese

At the time the EE REDOX model was developed for SB3 [24, 25], further investigation into the role of oxidized Mn species (+4, +5, +6, and +7) in the feed was suggested. Higher manganese concentrations had been experienced in the early projections of SB4 compositions. During non-radioactive melt rate testing of SB4 feed simulants, Equation 9 and Equation 10 predicted a REDOX target of $Fe^{2+}/\Sigma Fe$ of 0.2, but actual SB4 produced glasses that were overly oxidized, $Fe^{2+}/\Sigma Fe \sim 0$ (overly oxidized). These overly oxidized feeds foamed and the copious amounts of foam adversely impacted melt rate. At this point the EE REDOX model parameters were reinvestigated and it was determined the high nitrate in DWPF SB4 feeds was reoxidizing divalent manganese in the melter feeds during the denitration reactions in the cold cap. Therefore, the manganese in the cold cap is likely Mn^{+7} and not Mn^{+4} as assumed in Equation 9 and Equation 10.

Therefore, the 2003 EE REDOX model was refit in 2007 [30] with a factor of 5 for the manganese EE transfer in order to avoid foaming in high manganese containing feeds:

Equation 13
$$\frac{Fe^{2+}}{\Sigma Fe} = f\left[\left(2[F]+4[C]+4[O_T]-5[N]-5[Mn]\right)\frac{45}{T}\right] = f\left[\xi\right]$$

where f = indicates a function
[F] = formate (mol/kg feed)
[C] = coal (carbon) (mol/kg feed)
$[O_T]$ = $oxalate_{Total}$ (soluble and insoluble) (mol/kg feed)
[N] = nitrate + nitrite (mol/kg feed)
[Mn] = manganese (mol/kg feed)
T = total solids (wt%)

and

Equation 14
$$\frac{Fe^{+2}}{\sum Fe} = 0.2358 + 0.1999\xi$$

with an adjusted R^2 = of 0.81 and a RMSE of 0.0704.

The $Fe^{2+}/\Sigma Fe$ predictions from the Electron Equivalents model given above were fitted to measured REDOX data generated from the DWPF melter from SME Batch 224, to data generated by the Savannah River Technology Center (SRTC) now Savannah River National Laboratory (SRNL) mini-melter, and to data from the SRTC Slurry-fed Melt Rate Furnace (SMRF).[§]

1.6 DWPF Nitric/Formic Flowsheet with Oxalate, Coal, Higher Manganese, Antifoam, and Ar Bubbling

In 2012, an EE was needed for the antifoam feed additive [31]. Antifoam is an organic chain structure composed of methyltrisiloxane (MTS) end groups and a center polymer chain of varying length (8 to 12 polyethyleneoxide or PEO groups), and the EE term must be based on the number of carbons in each part of the organic group and their relative EE term. This is the same strategy used to fit a carbon term for coal in the EE REDOX model but the antifoam molecule contains carbons of different oxidation states so it is more complex.

[§] This data can be found in Appendix B.

The MTS end groups of the antifoam molecule have 7-8 carbons of -4 charge. The 8 chain PEO groups have 16 carbons of -1 charge. The 12 chain polymers have 24 carbons of -1 charge. Since the ratio of the 8:12 polymer chains is 90%:10%, there are 16.8 carbons of -1 charge in the weighted polymer chain. The 8 carbons in the MTS (if the MTS groups are assumed to be octa-MTS instead of hepta-MTS) yield a total of 24.8 carbons in the antifoam organic molecule (sum of 0.9*16 + 0.1*24). The -1 carbons of the PEO exchange 5 EE's per carbon to oxidize to CO_2 in the melter. The -4 carbons of the octa-MTS exchange 8 EE's per carbon to oxidize to CO_2 in the melter. Experimentation and modeling [31] have shown that the MTS's cleave off the antifoam during processing and do not participate in reduction of the melt pool. Therefore, the EE of the PEO groups are 16.8/24.8 carbons times 5 EE per carbon which yields a total EE transfer term of +3.39 per mole/kg of carbon as shown in Equation 15.

Equation 15

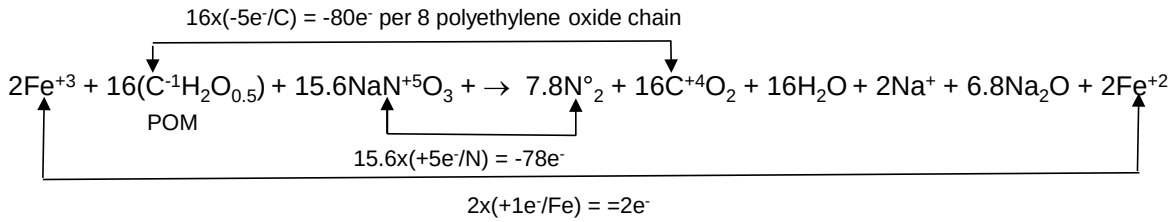

In order to use Equation 15 correctly the following conversions are made so that

mg/kg of antifoam→mg/kg of total carbon in antifoam→mol/kg of total carbon in antifoam.

This method of conversion from antifoam to mol/kg of carbon was chosen because the DWPF data available were in mg/kg of antifoam calculated from how many gallons of antifoam had been measured per SME batch. Also sealed crucible studies, performed after known amounts of antifoam had been added, were available in mg/kg of antifoam. The DWPF data were available as the measured Total Organic Carbon (TOC) in mg/kg of carbon. The mg/kg of carbon from the antifoam was determined by subtracting the carbon contribution from formic acid, oxalate/oxalic acid, and coal. Modeling was performed using mol/kg carbon derived from gallons of antifoam used and from TOC measurements.

Experimentation and modeling [32] have shown that the antifoam PEO's are 80-100% effective in melt pool reduction. The modeling performed for the REDOX model for antifoam suggests that the efficiency is 85%. Therefore, 85% of +3.39 EE yields an overall EE transfer of +2.88 per mol/kg of carbon from antifoam compared to +2 for formic acid and +4 for oxalate and coal. Having an antifoam term in the REDOX model may allow antifoam to be used as a reductant source while also controlling feed foaming. More information has been obtained on how antifoam degrades [33, 34] and the antifoam term may be revised in the future. This would alter the antifoam term slightly but then also alter the efficiency factor that was fit to experimental data so the impact of the overall term on REDOX would remain the same.

In addition, the DWPF had begun to sparge the melt pool with Ar bubblers and the impact of the Ar bubbling on REDOX was needed. There is an additive impact on the melt pool REDOX from the argon bubbling. Argon degasses or sparges the oxygen from the melt. Thus, REDOX is a function of both the oxidants and reductants in the melt pool and the Ar sparging. While Ar is an inert gas, Ar replaces the free oxygen in a glass. This process also occurs when inert gasses are used to sparge the oxygen or other gasses out of solutions, molten metals, or glasses. The REDOX equilibrium in a glass melt can be represented by

Equation 16

$$Fe^{3+}_{melt} + \frac{n}{2} O^{2-}_{melt} \leftrightarrow Fe^{2+}_{melt} + \frac{n}{4} O_{2\ melt}$$

where n = the number of electrons transferred
O^{2-} = the oxygen ion activity or basicity of the melt
O_2 = the physically dissolved oxygen in the holes of the network structure
Fe^{3+} = oxidized iron species in the melt
Fe^{2+} = reduced iron species in the melt

The REDOX-oxygen balance equation is written as reversible; going from the RHS to the LHS is the reduction of ferric to ferrous iron and going from LHS to RHS is the oxidation of ferrous to ferric iron. Since the DWPF melt pool reductants shift the equilibrium to the RHS where dissolved oxygen exists in the glass, it is the dissolved oxygen on the RHS of this equation that is being displaced by the Ar in the melt pool. This is because the free oxygen on the RHS of the equation is being sparged out and the equilibrium between the RHS and the LHS no longer exists, driving the equilibrium to the RHS. Therefore, O_2 must be provided by either (1) additional melt pool oxidants (the theory of targeting a more oxidizing REDOX target to compensate for the Ar sparging) or (2) using a mixing valve to admix small amounts of air into the argon while sparging. Reference 31 provides the calculations of Ar-air mixtures that would be acceptable if the latter route is desired.

Measurement of the REDOX of DWPF pour stream (PS) samples (with and without Ar bubbling) and measurement of a simulated SB6 feed that was Ar bubbled during the feed-to-glass transformation in a sealed crucible inside an Ar bubbled oven demonstrated that the argon bubbling impact is a linear constant of $Fe^{+2}/\Sigma Fe$ of ~0.1. Therefore, it was recommended in Reference 31 that targeting a chemical REDOX of 0.1 should yield a realized $Fe^{+2}/\Sigma Fe$ of ~0.2. While there is no EE term that can be developed for Ar sparging, an "effective offset" term has been added to the REDOX model, which is 0.1, to account for Ar degassing.

The DWPF REDOX model then takes the form

Equation 17

$$\frac{Fe^{2+}}{\Sigma Fe} = f\left[\left(2[F] + 4[C] + 4[O_T] + 3.39 * eff\,[C_A] - 5[N] - 5[Mn]\right)\frac{45}{T}\right] = f\left[\xi_A\right]$$

where f = indicates a function
[F] = formate (mol/kg feed)
[C] = coal (carbon) (mol/kg feed)
$[O_T]$ = $oxalate_{Total}$ (soluble and insoluble) (mol/kg feed)
$[C_A]$ = carbon from antifoam (mol/kg feed)
eff = effective antifoam impact = 0.85
[N] = nitrate + nitrite (mol/kg feed)
[Mn] = manganese (mol/kg feed)
T = total solids (wt%)

When the REDOX data generated were fit as a linear function of ξ_A they fell within the confidence bands of the 2007 EE model (Equation 13 and Equation 14) and so the slope and intercept were not refit. This gives the form of the DWPF REDOX model with an antifoam term (the 2012 model) as:

Equation 18 $$\frac{Fe^{2+}}{\Sigma Fe} = 0.2358 + 0.1999\xi_A$$

The impact of Ar sparging on REDOX was quantified and the Ar adjusted DWPF model takes on the form:

Equation 19 $$\frac{Fe^{2+}}{\Sigma Fe} = 0.2358 + 0.1999\xi_A + 0.1_{Ar}$$

1.7 Electron Equivalents Term for Nitric Acid-Glycolic Acid (NG) Flowsheet

It is assumed that glycolic acid forms a sodium glycolate salt during reflux in the SRAT similar to the manner in which formic acid forms a sodium formate salt during reflux in the SRAT. The glycolic acid flowsheet is similar to the formic acid flowsheet in that it buffers around a pH of 4 and the amount of free acid is a function of the final pH of the SRAT, i.e. a portion of the glycolate may exist as glycolic acid. Whether glycolate exists as a salt or as the acid does not affect the REDOX balance calculation. The simplest reaction for sodium glycolate being oxidized by sodium nitrate is given as Equation 20, assuming that all of the carbon oxidizes to CO_2 as do all the other reductants in the DWPF REDOX model [31].

Equation 20

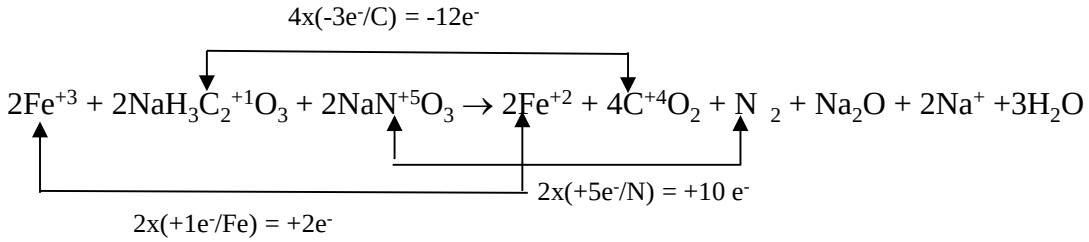

Equation 20 demonstrates that 3 EE are lost per carbon for a total of 6 EE per mole of glycolate oxidized. In reality the carbons in glycolate are approximately +2 and a 0, for an average of +1 per carbon as indicated in Equation 20. Therefore, if the equation were written with the 0 carbon losing 4 EE to oxidize to +4 carbon and the +2 carbon losing 2 EE to oxidize to +4 carbon it would still give an EE of (4+2=) 6 EE per mole of glycolate.

1.8 DWPF Interim Nitric Acid-Glycolic Acid (NG) REDOX Model

The development of an EE term for the NG flowsheet had been problematic due to variability in the glycolate measurement in the feed. Glycolate measurements in SRAT/SME feeds had been problematic until SRNL Analytic Development Division (ADD) developed a caustic quench method [35] to improve glycolate analysis. Until accurate glycolate measurements were available it was difficult to develop a glycolate term for the REDOX model.

The development of an EE term for the NG flowsheet was also problematic due to variability in the determined $Fe^{+2}/\Sigma Fe$ which was found to be highly dependent on the type of closed (sealed) crucible (CC) method utilized to produce glass for REDOX measurement [36]. In Reference 36, the CC_{ramp}, CC_{Ar} and Closed Crucible with Off-Gas (CCOG) variants of the CC method were shown to be unsuitable for REDOX modeling. The CC_{hot} which requires an 1150°C hot insertion of the CC into the furnace, has

been and continues to be the most reliable method for $Fe^{2+}/\Sigma Fe$ determination of SRAT/SME feeds. The CC_{hot} methodology was supplemented by Melt Rate Furnace (MRF) tests of the same feeds. The MRF tests gave comparable $Fe^{+2}/\Sigma Fe$ ratios to the CC_{hot} tests [36].

For some simulated feeds, i.e., SB4 and SB6 [30, 36], the use of a refractory frit like Frit 418 was shown to give irreproducible $Fe^{+2}/\Sigma Fe$ ratio determinations even with CC_{hot}. This was because the glass in the CC_{hot} test was at too high a viscosity and thus inhibited convection in the crucible which produced an inhomogeneous glass. Inhomogeneous glass gives non-uniform $Fe^{+2}/\Sigma Fe$ measurement results. To ensure that the glass viscosity variable was controlled, the latest revision of the REDOX procedure [44] was adjusted to require that the SRAT-frit mixture being tested in CC_{hot} have a calculated viscosity of 60 poise or less at 1150°C. This was the viscosity found to provide a homogeneous glass during SB4 testing [30]. If the SRAT-frit mixture is calculated from the algorithm given in Reference 37 to have a viscosity of >60 poise, $LiBO_2$ is now required to be added as a flux that does not impact the overall REDOX of the mixture.

A Mn term of zero was chosen for the interim REDOX model as experimentation documented in Reference 36 had shown the presence of a Mn^{2+} species in the NG flowsheet sludge samples dried at 40°C and in deposits found in the Cold-cap Evaluation Furnace (CEF) feeds [38 , 41]. This experimentation included analyses by XRD that were performed on air dried SRAT/SME products and High Temperature X-Ray Diffraction (HTXRD) [39] on the NG flowsheet for comparison to HTXRD's performed on the NF flowsheet.[11,40] In addition, Heat and Stop (H&S) crucible studies had been performed where the SME product is heated at a given temperature for 1 hour and the reaction stopped at that temperature so that the SME product phases could be identified by XRD. Heat and stop samples were heat treated to 40°C, 300°C, 500°C, and 775°C and then the phases were identified by XRD.[41] The details of the HTXRD and H&S are given elsewhere [39,41] and reported in Reference 36. Since these experiments showed that the incoming manganese species from the SME is +2 then the manganese EE term became zero in the NG flowsheet interim REDOX model.

Based on the combined acceptable CC_{hot} and MRF analyses given in Reference 36, it was recommended that the DWPF use the 2012 REDOX model slope and intercept from Reference 31 with a glycol EE of 6 and Mn EE=0 as an *interim* REDOX model for the NG flowsheet at 100-125% acid stoichiometry as indicated in Equation 21 below.

Equation 21

$$\xi_{A\text{-}gly} = \left[\left(2[F] + 4[C] + 4[O_T] + 3.39 * eff\,[C_A] + 6[Gly] - 5[N] - 0[Mn] \right) \frac{45}{T} \right]$$

where
- [F] = formate (mol/kg feed)
- [C] = coal (carbon) (mol/kg feed)
- $[O_T]$ = $oxalate_{Total}$ (soluble and insoluble) (mol/kg feed)
- $[C_A]$ = carbon from antifoam (mol/kg feed)
- eff = effective antifoam impact = 0.85
- [Gly] = glycolate (mol/kg feed)
- [N] = nitrate + nitrite (mol/kg feed)
- [Mn] = manganese (mol/kg feed)
- T = total solids (wt%)
- $\xi_{A\text{-}gly}$ = EE term with antifoam and glycolate

and

$$\frac{Fe^{2+}}{\Sigma Fe} = 0.2358 + 0.1999\xi_{A-gly}$$

Note that Equation 21 can be used with or without the Ar bubbling term offset of 0.1. The slope and intercept in Equation 21 from References 31and 30 are the same because that is the slope and intercept that were used to determine the effective antifoam impact term of 0.85. In other words, the antifoam data were not used as model data in References 31 and 30. If the antifoam data are included there is some improvement in the model fit due to the high leverage points that the antifoam data provided at both high and low REDOX. For comparisons to the improved NG REDOX data in Section 3.4 the fit to the 182 datapoints was used since the antifoam data had the higher REDOX leverage points.

Note that an EE of 6 for glycolate is the theoretical number (see Section 1.7) of electrons transferred when a mole of glycol in the feed converts to CO_2 in the off-gas in the DWPF melter. A de minimis of 800 mg/kg,which is equivalent to 0.03267 mol/kg of carbon from antifoam in the feed, essentially reduces the antifoam term in the above equation to near zero. If lower acid stoichiometries are used in the NG flowsheet than those evaluated in Reference 36 (100-125% acid stoichiometry) or in this study (76.9 to 123.2% KMA basis or 107-134 Hsu basis), the validity of the Mn EE=0 may need to be re-evaluated. Where the KMA acid basis is given in Reference 28 and the Hsu acid basis is given in Reference 42.

2.0 Experimental Procedure

A matrix of NG melter feed preparations [43], which targeted various REDOX ranges beyond the typical operating range, was tested in closed (sealed) crucible melts following the ITS-0052 REDOX procedure as modified by the inclusion of the calculated batch viscosity [44]. Once the NG feed-to-glass conversions were complete, the glass was dissolved following the Baumann methodology (ITS-0042) [45, 46] and colorimetric measurements of the $Fe^{2+}/\Sigma Fe$ ratio were made to generate data necessary to update or validate the interim NG REDOX model. Optical microscopy examinations of the glasses were performed to ensure glass homogeneity, and the acceptable sample data were added to the historic REDOX database.

2.1 Preparation of Simulant

Both SRAT/SME product feeds from thirteen experiments (ten SRAT-only and three SME) were utilized to provide additional leverage points to validate the interim NG REDOX model. The different experiments were designed to produce products with REDOX values across the REDOX measurement spectrum (from <0.1 to ~0.5 $Fe^{2+}/\Sigma Fe$), not just within the normal DWPF operational range. Figure 2-1 shows a visualization of the expanded test matrix, plotted as a function of calculated acid stoichiometry versus the percentage of reducing acid out of the total acid added. Predicted REDOX values were calculated based on the analytical measurements of the products and compared to the measured REDOX values of each glass.

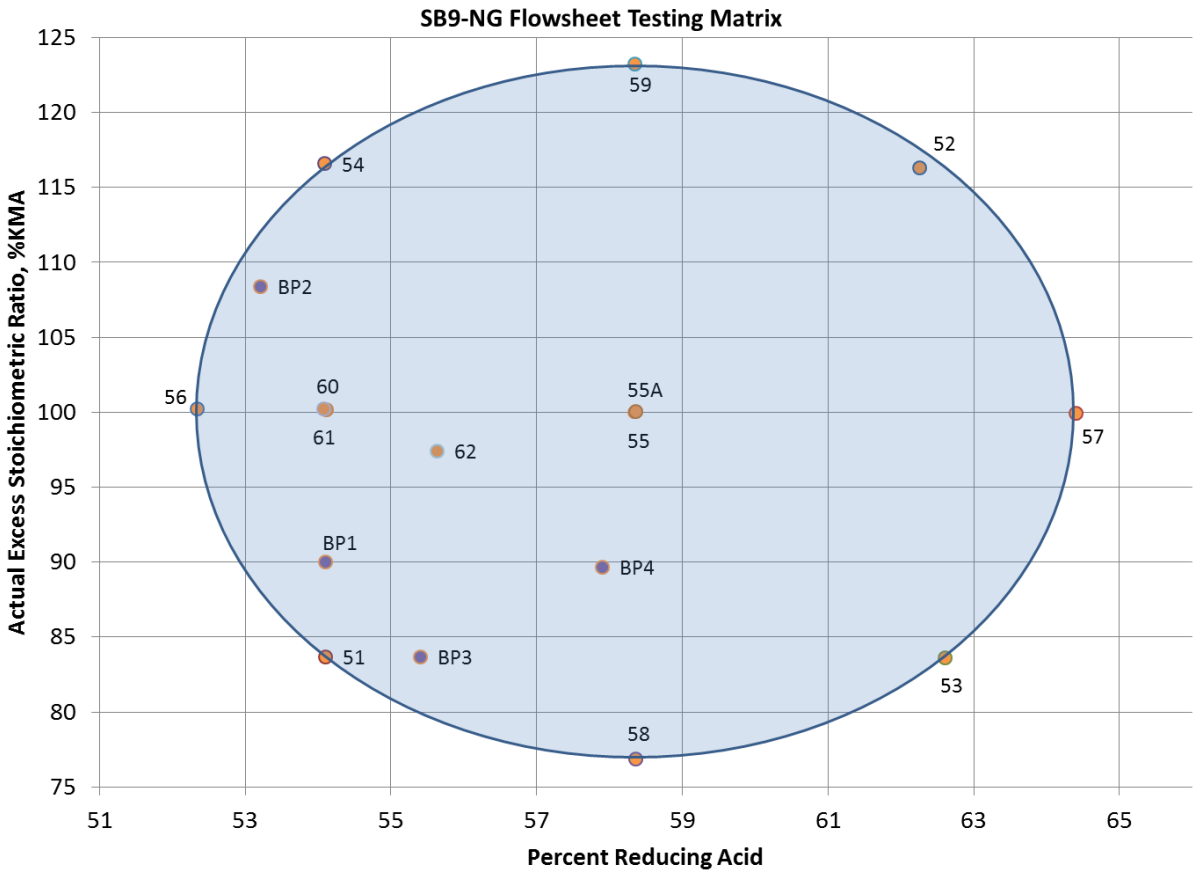

Figure 2-1. NG Flowsheet Matrix of Experiments as a Function of Acid Stoichiometry versus Percent Reducing Acid with Run Identification Values

Note: labels are equivalent to SB9-NG experiment. Identifications such as 52 is the experiment SB9-NG-52. The blue circle represents the outer most range of acid combinations tested [43]. Some samples lie on the outer extreme of the circle and some lie within the circle.

Four blended products were formulated from some of the SRAT products (labelled as BP#). These blends were utilized to fill in data within the operating range. Table 2-1 details which SRAT products were combined and in what ratios to produce the blends with the desired targeted REDOX values.

Table 2-1. Blended Product Formulations

	Blended Product			Blend Component 1		Blend Component 2	
ID	Calculated KMA	Calculated Hsu	Calculated PRA	ID	Blend %	ID	Blend %
BP 1	90.0	94.1	54.1	SB9-NG 51	80.85	SB9-NG 54	19.15
BP 2	108.4	113.3	53.2	SB9-NG-56	50	SB9-NG 54	50
BP 3	83.7	87.5	55.4	SB9-NG 51	84.71	SB9-NG 53	15.29
BP 4	89.6	93.7	57.9	SB9-NG 51	63.11	SB9-NG 57	36.86

Note: KMA is Koopman Minimum Acid stoichiometry; PRA is Percent Reducing Acid

2.2 Closed Crucible Hot Insertion (CC_{hot})

The procedure for CC_{hot} [44] calls for vitrification of sufficient SRAT/frit or SME product to fill the chosen crucible (typically a 100mL alumina crucible) to approximately 2/3 full (between 60 and 70mL). The exact amount is calculated by a formula given in the latest revision of the REDOX procedure [44] and is provided for each sample in the associated electronic laboratory notebook (ELN) given in Section 2.3.

The SRAT/frit mixture in the crucible is dried in an oven at 50±5°C until it reaches a water mass loss of 90-95%. The dried sludge is then stirred to homogeneity and the lid is sealed onto the crucible using a nepheline ($NaAlSiO_4$) gel. The gel is dried and the crucible is preheated at 70°C for at least 30-45 minutes to prevent thermal shock. The preheated crucible is placed directly into a hot furnace at 1150°C. Once the oven recovers temperature from the process of inserting crucibles, the samples are held for one hour and then removed to a pan of sand or a refractory brick to quench cool in air. When the samples have cooled, the glass is broken out of the crucible and pieces are isolated from the interior of the glass, away from the surface exposed to the atmosphere or the surface in contact with the alumina crucible. The surface and interior faces of the remaining glass are imaged via optical microscope and/or SEM to examine the glass homogeneity and extent of crystallization. These interior glass samples are then analyzed for REDOX measurements according to the latest revision of the REDOX procedure [44]. Often a different top layer, which looks like a cold cap, can be observed in the CC_{hot} experiments. A cold cap type reaction layer was also noted in SB4 testing [30]. These regions should also be avoided when sampling for $Fe^{+2}/\Sigma Fe$ analyses.

A known issue with the REDOX procedure includes failing to dry the sample slurry sufficiently to reduce the amount of steam escaping when the insertion into the hot furnace at 1150°C is performed. Large amounts of steam from the insufficiently dried sample can cause the lids to pop off the crucible even though they are sealed with a nepheline-based gel. Exposing the SRAT/frit mixture to the oxygen in the air any time after the crucible is placed in the 1150°C oven, releases reactive off-gas species before they are able to react and exposes the feed to air. This yields an invalid REDOX measurement that cannot be used. The procedure was revised to dry to an almost dry consistency (90-95% water loss) to minimize the chances for crucible lids to pop off due to excess release of steam. However, a small amount of water is necessary to complex with the other gases during the feed-to-glass transition in the crucible and to mimic the reactions that occur in a slurry fed melter cold cap. The revised procedure was used to generate the enhanced REDOX data used in this study. An additional issue, which has been observed during experimentation, is the loading of too many samples at one time into an 1150°C oven such that the recovery of the oven temperature is delayed. Overloading furnaces also reduces the insertion temperature that the later crucibles experience as the furnace has significantly cooled by the time they are inserted. Ideally only one sample or a few samples (1-3) should be loaded at any given time.

The ITS-00520 procedure requires that the REDOX procedure be repeated 3 times with the same SRAT/frit aliquots in 3 different crucibles. The REDOX ratio is then determined by the Reference 45 methodology which is the same as the Process Science Analytic Laboratory (PSAL) REDOX procedure.[46] The glass from each of the 3 crucibles is dissolved once and the Fe^{2+} and total Fe are read twice colorimetrically which are referred to later in this document as A/B analytic pairs. The Fe^{2+} and ΣFe should be reported separately. For 3 viable crucible melts, i.e. those that the lids have not popped and are homogeneous, there should be 6 pairs of Fe^{2+} and ΣFe measurements. This is done because the REDOX procedure gives a “noisy” response and by performing triplicate analyses, obvious outliers can be discarded before REDOX modeling.

2.3 Quality Assurance

All the data reported in this study were developed under the quality assurance given in the Task Technical and Quality Assurance Plan (TTQAP) SRNL-RP-2012-00762 [47]. The research program and task plan were developed to address HLW-DWPF-TTR-2013-0003 [48] entitled "Phase II – Nitric-Glycolic Acid Flowsheet Testing Technical Task Request" and X-TTR-S-00024 [49] entitled "Bounding Alternate Reductant Testing/Chemistry and REDOX Definition." Task 2c in Reference 48 requested that a REDOX model appropriate for the NG flowsheet be developed. The 2014 TTR requested that issues with glycolate measurement be resolved and that a best fit REDOX model be developed.

The details of the CC_{hot} REDOX studies are given in the following ELN:

- M. S. Williams "Completion of Interim REDOX Model Incorporating the Nitric-Glycolic Flowsheet," U.S. Dept. of Energy, Savannah River National Laboratory, Aiken, SC, ELN# I7770-00157-14, 2017.
- M. S. Williams "Completion of Interim REDOX Model Incorporating the Nitric-Glycolic Flowsheet – Volume 2," U.S. Dept. of Energy, Savannah River National Laboratory, Aiken, SC, ELN# I7770-00157-16, 2017.

Requirements for performing reviews of technical reports and the extent of review are established in manual E7 2.60. SRNL documents the extent and type of review using the SRNL Technical Report Design Checklist contained in WSRC-IM-2002-00011, Rev. 2. Tommy Edwards performed the E7 review of Carol Jantzen's sections and Cory Trivelpiece performed the E7 review of Tommy Edwards' sections.

3.0 Results and Discussion

3.1 Feed Analyses and Weight Percent (wt%) Solids

Table 3-1 details the anion concentrations analyzed in the melter feeds used for NG REDOX testing. Table 3-1 also contains the % acid stoichiometry on both the KMA [28] and Hsu [42] bases. Table 3-2 contains the average weight percent total solids measurements of each feed on a SME basis [43]. The concentrations given in Table 3-1 get normalized to the ratio of 45/T where T represents the total SME solids (Table 3-2). This normalization corrects the concentrations in the feeds to a consistent wt% solids so that the impacts of more dilute versus more concentrated feeds does not impact REDOX modeling [19, 24, 25, 30, 31].

3.2 Variability of REDOX Replicate Measurements

Figure 3-1 provides a plot of the REDOX measurements for the SB9 glasses of interest. The measurements are grouped by glass ID, crucible label, and duplicate analysis. An immediate observation is how repeatable the analytical measurements are for each of the crucibles (A/B pairs) with most of the variation in the REDOX measurements for a glass being due to differences among the three crucible tests.

Table 3-1. Concentrations of Anions* (mol/kg slurry basis)

SB9-NG Run #	Nitrate	Glycolate	Oxalate	Formate	Antifoam	Manganese	Acid in Excess Stoichiometric Ratio (%)	
							KMA	Hsu
SB9-NG-51	0.693	0.460	0.099	0.014	0.025	0.203	83.7	87.5
SB9-NG-52	0.813	0.770	0.074	0.014	0.031	0.165	116.3	121.5
SB9-NG-53	0.587	0.496	0.100	0.027	0.025	0.196	83.6	87.4
SB9-NG-54	0.936	0.630	0.067	0.000	0.035	0.184	116.6	121.8
SB9-NG-55	0.742	0.556	0.093	0.000	0.028	0.208	100.0	104.5
SB9-NG-55A	0.888	0.613	0.088	0.000	0.01	0.147		
SB9-NG-56	0.849	0.512	0.094	0.000	0.025	0.191	100.2	104.7
SB9-NG-57	0.701	0.719	0.093	0.000	0.025	0.196	99.9	104.4
SB9-NG-58	0.623	0.482	0.112	0.021	0.015	0.200	76.9	80.3
SB9-NG-59	1.024	0.768	0.070	0.017	0.023	0.131	123.2	128.8
SB9-NG-60	0.823	0.541	0.080	0.000	0.021	0.169	100.2	104.7
SB9-NG-61	0.806	0.471	0.112	0.000	0.025	0.187	100.2	104.7
SB9-NG-62	0.813	0.568	0.072	0.013	0.028	0.161	97.4	103.3
BP-1	0.739	0.492	0.092	0.012	0.027	0.200	90.0	94.1
BP-2	0.893	0.571	0.080	0.000	0.030	0.187	108.4	113.3
BP-3	0.677	0.466	0.099	0.016	0.025	0.202	83.7	87.5
BP-4	0.696	0.556	0.097	0.009	0.025	0.201	89.6	93.7

* F^-, Cl^-, and PO_4^{-3} are all below detection limit of <500 mg/L

Table 3-2. Weight Percent Total Solids on a SME Basis.

SB9-NG Run #	Wt% Solids
SB9-NG-51	46.0
SB9-NG-52	40.0
SB9-NG-53	45.0
SB9-NG-54	41.8
SB9-NG-55	47.0
SB9-NG-55A	31.1*
SB9-NG-56	45.7
SB9-NG-57	46.1
SB9-NG-58	45.4
SB9-NG-59	28.6*
SB9-NG-60	46.0
SB9-NG-61	37.1
SB9-NG-62	37.2
BP-1	45.1
BP-2	43.7
BP-3	45.8
BP-4	46.0

* samples with the highest acid stoichiometry which were diluted to low wt% solids intentionally to fix rheology problems [43]

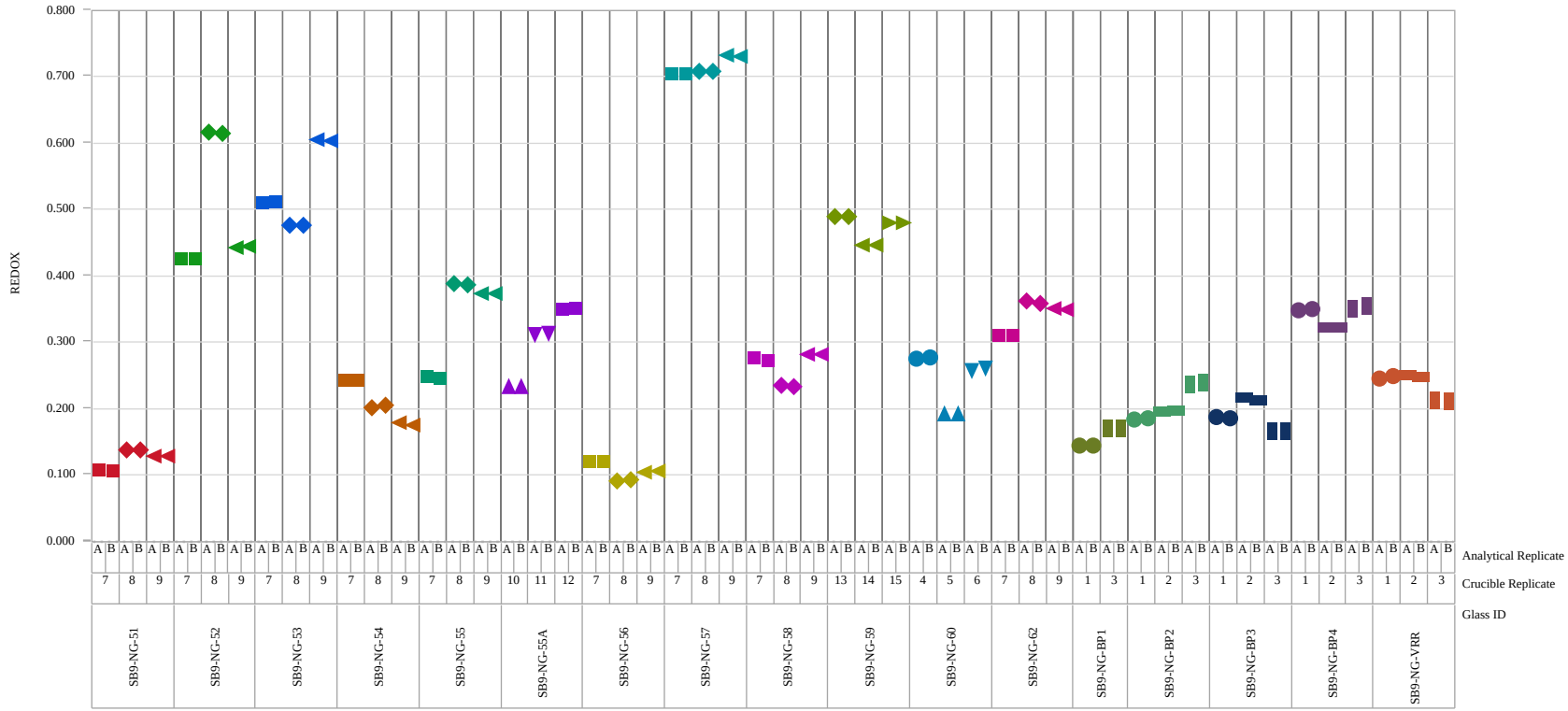

Figure 3-1. REDOX Measurements by Glass ID, Crucible Label, and Duplicate (A,B) Analysis.

Variability between crucibles is a function of the subtle variations in conditions for each; for example, the exact level of dryness of the material, the efficiency with which the material was homogenized before sealing, the position of the crucible in the oven, the individual fluctuations in thermal convection once molten, and the individual cooling rate of each crucible. The analytic variability within the crucible is a function of homogeneity of the glass once it has cooled. To minimize the effects that inhomogeneity in a single crucible can have, only REDOX analyses from glasses that appear homogeneous under microscopic examination are considered acceptable for modeling. Inhomogeneities in the glass lead to higher variability as the Fe^{2+} to Fe^{3+} concentrations can vary drastically within the sample. The acceptability of each glass is determined by examination with a Dino-Lite digital microscope. Examples of acceptable and unacceptable glasses from the recent SB9-NG glass study as well as the blended product studies are shown in Figure 3-2 A-D; images of all glasses are in the ELN given in Section 2.3. Samples that show uniformity in color and lack of crystallization in the interior are acceptable for use in the REDOX modeling. Unacceptable glasses are shown in images A and C and acceptable glasses are shown in images B and D.

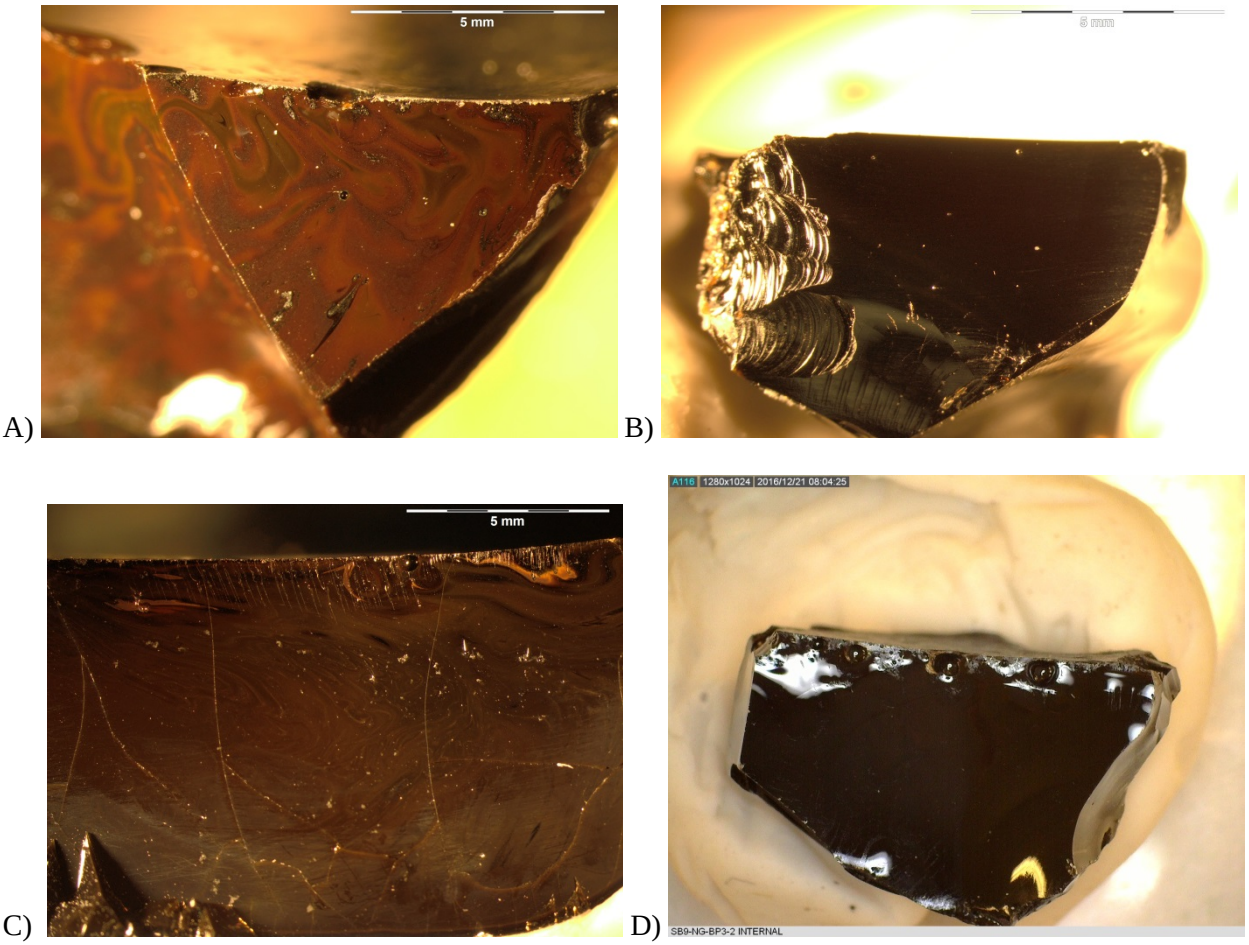

Figure 3-2. Microscopic Images of Glass Interiors from Samples SB9-NG- A) 51-6, B) 55A-3, C) 59-6, and D) BP3.

3.3 NG Data for DWPF REDOX Model

3.3.1 Data for Modeling the NG Flowsheet

Figure 3-3 shows the average measured REDOX values for the recent SB9-NG testing in relation to the aforementioned test matrix. Table 3-3 shows the average measured REDOX values ($Fe^{+2}/\Sigma Fe$) in relation to the predicted values based on the compositional analyses of the SRAT/SME products. Note that all of the data, including potential modeling outliers, are being evaluated in this analysis.

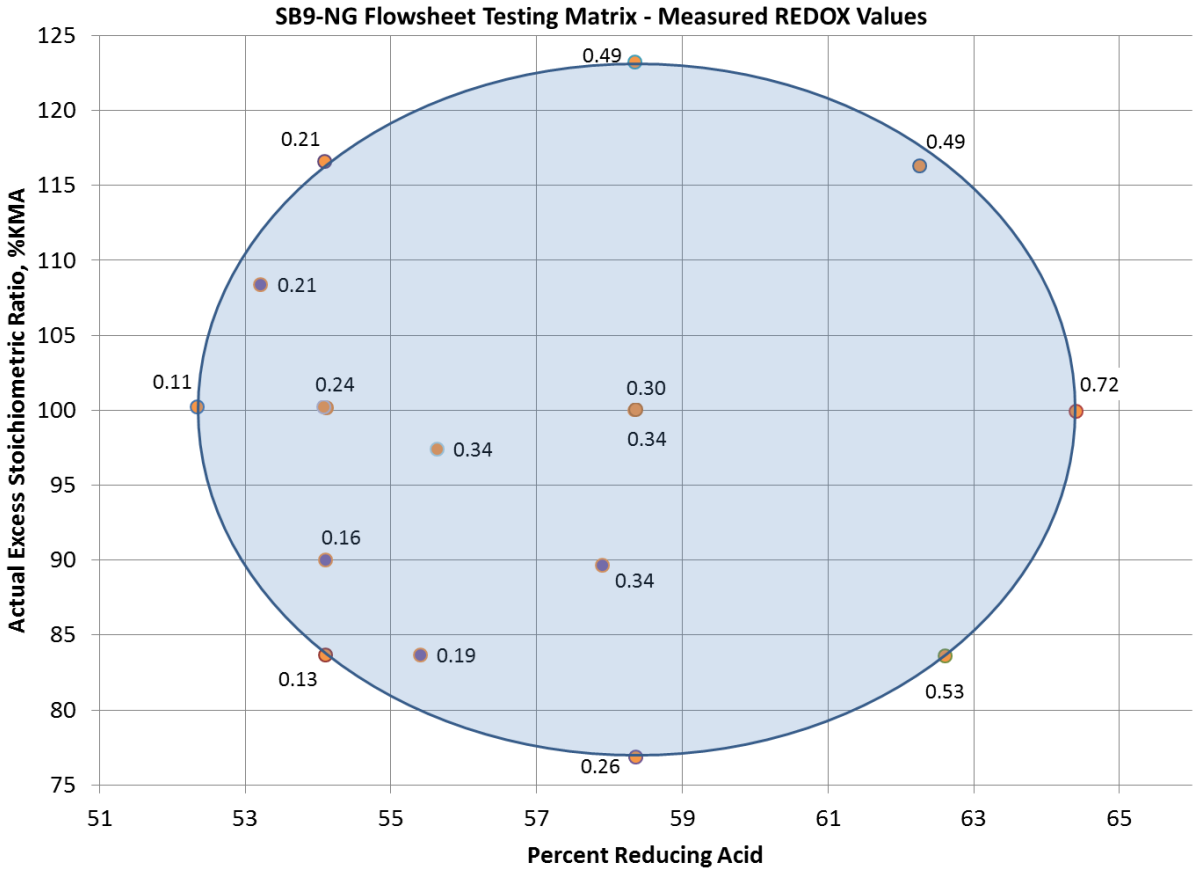

Figure 3-3. NG Flowsheet Matrix of Experiments as a Function of Acid Stoichiometry versus Percent Reducing Acid with Average Measured REDOX values.

Table 3-3. Predicted REDOX Values of NG Flowsheet Matrix.

SB9-NG Run #	**Predicted $Fe^{+2}/\Sigma Fe$ Using Analytical Measurements** from Feed Product Measurements After Processing	**Measured $Fe^{+2}/\Sigma Fe$**
SB9-NG-51	0.18	0.13
SB9-NG-52	0.41	0.49
SB9-NG-53	0.34	0.53
SB9-NG-54	0.11	0.21
SB9-NG-55	0.23	0.34
SB9-NG-55A	0.15	0.30
SB9-NG-56	0.08	0.11
SB9-NG-57	0.47	0.72
SB9-NG-58	0.29	0.26
SB9-NG-59	0.20	0.49
SB9-NG-60	0.13	0.24
SB9-NG-62	0.17	0.34
BP 1	0.18	0.16
BP 2	0.11	0.21
BP 3	0.22	0.19
BP 4	0.30	0.34

Note: shaded lines are low weight percent solids (<32 wt%) that are in the model range where the 45/T assumption is non-linear (see Figure 3-7)

The predicted REDOX values trend shows that the measured values go up as you go up and to the right across the matrix shown in Figure 3-3. This trend is reflected for the most part in the actual data. The values show how the REDOX is weighted in terms of both how much total acid you add to the system (KMA) and the ratio of reducing to total acid (PRA). There is a strong effect to the REDOX value as the PRA is increased. Considering the strong reducing nature and the high EE a single molecule of glycolate brings to the REDOX equation, this is to be expected. The effect from KMA is more subtle and is even wiped out as the PRA dominates at the highest region of the matrix.

Figure 3-4 provides a plot of the average REDOX results for each crucible for each glass. This leads to three values for each glass except SB9-NG-BP1, for which only two crucible melts were performed. Also shown for each glass is a 95% confidence diamond for the average REDOX value for each test glass. The height of the diamond for a glass is determined by the number of crucibles used for the glass and the variation among the average REDOX results across the crucibles for the glass. Since 3 crucibles were typically used for each glass, the heights of the mean diamonds for the glasses provide insight into the variation in the REDOX results for these glasses. Specifically, more variation is seen in SB9-NG-52, SB9-NG-53, SB9-NG-55, SB9-NG-55A, and SB9-NG-60. The larger height of the mean diamond for SB9-NG-BP1 is due to its having used only 2 crucible results.

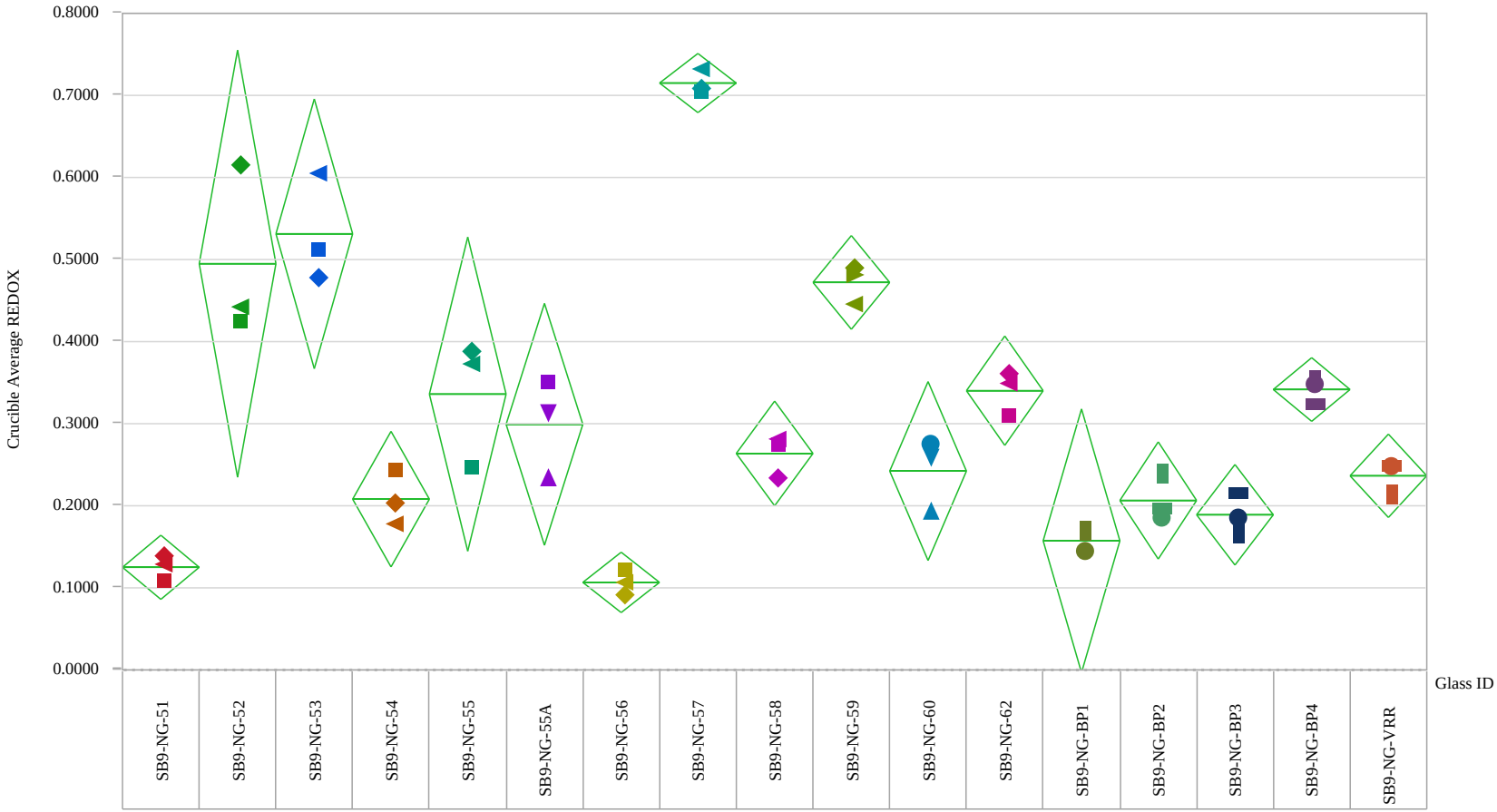

Figure 3-4. Plot of the Average REDOX Values by Crucible by Glass ID.

An analysis of variance (ANOVA) was conducted for these data to investigate for differences among the average REDOX values for these study glasses. This one-way ANOVA is conducted under the assumption that the scatter in the replicate crucible results is common across all of the test glasses. The ANOVA results are provided in Table 3-4; these indicate that there are differences among the average REDOX values for these test glasses at a statistical significance level of 5%. The RMSE, the estimate of the standard deviation in the crucible results common to all of the study glasses, is 0.044.

Table 3-4 ANOVA Results.

Oneway Anova

Summary of Fit

Rsquare	0.950148
Adj Rsquare	0.925978
Root Mean Square Error	0.044494
Mean of Response	0.312798
Observations (or Sum Wgts)	50

Analysis of Variance

Source	DF	Sum of Squares	Mean Square	F Ratio	Prob > F
Glass ID	16	1.2451897	0.077824	39.3101	<.0001*
Error	33	0.0653319	0.001980		
C. Total	49	1.3105216			

To explore these differences in more detail, an additional statistical evaluation was conducted: the Tukey-Kramer HSD (honestly significant difference) test that is sized for all differences among the means.

Table 3-5. Tukey-Kramer HSD Test Results: Connecting Letters Summary.

Sample ID	Level						Average REDOX
SB9-NG-57	A						0.715
SB9-NG-53		B					0.531
SB9-NG-52		B					0.495
SB9-NG-59		B	C				0.472
SB9-NG-BP4			C	D			0.342
SB9-NG-62			C	D			0.340
SB9-NG-55				D			0.336
SB9-NG-55A				D	E		0.299
SB9-NG-58				D	E		0.264
SB9-NG-60				D	E	F	0.242
SB9-NG-VRR				D	E	F	0.237
SB9-NG-54				D	E	F	0.208
SB9-NG-BP2				D	E	F	0.206
SB9-NG-BP3					E	F	0.189
SB9-NG-BP1					E	F	0.157
SB9-NG-51						F	0.125
SB9-NG-56						F	0.107

Table 3-5 presents the average REDOX values sorted from largest to smallest. Glass ID's not connected by same letter are significantly different.

Thus, SB9-NG-57, with the largest REDOX value, is different from all of the other glasses. The next three glasses in the table (SB9-NG-53, SB9-NG-52, and SB9-NG-59), while not different from each other, the first two glasses in this set are different from all of the other glasses with SB9-NG-59 also being a part of the "C" group. All of the glasses labeled as "C" form a group (i.e., their average REDOX values do not appear to be statistically different from one another). These "C" glasses have mean REDOX values

that are not statistically different from one of the glasses that falls in the “B” group and a couple of glasses within the “D” grouping. However, the top glass in the “C” group does differ from all of the “D” glasses. Similar conclusions can be made for the glasses in the “D” group. Some have means that are not statistically different from the means of some of the “C” glasses nor from the means of some of the “E” and some of the “F” glasses. Finally, the last two “F” glasses differ from all of the “D” and “E” glasses as well as glasses in the “A”, “B”, and “C” groups. Figure 3-5provides a plot of the sorted REDOX values that reflect these results.

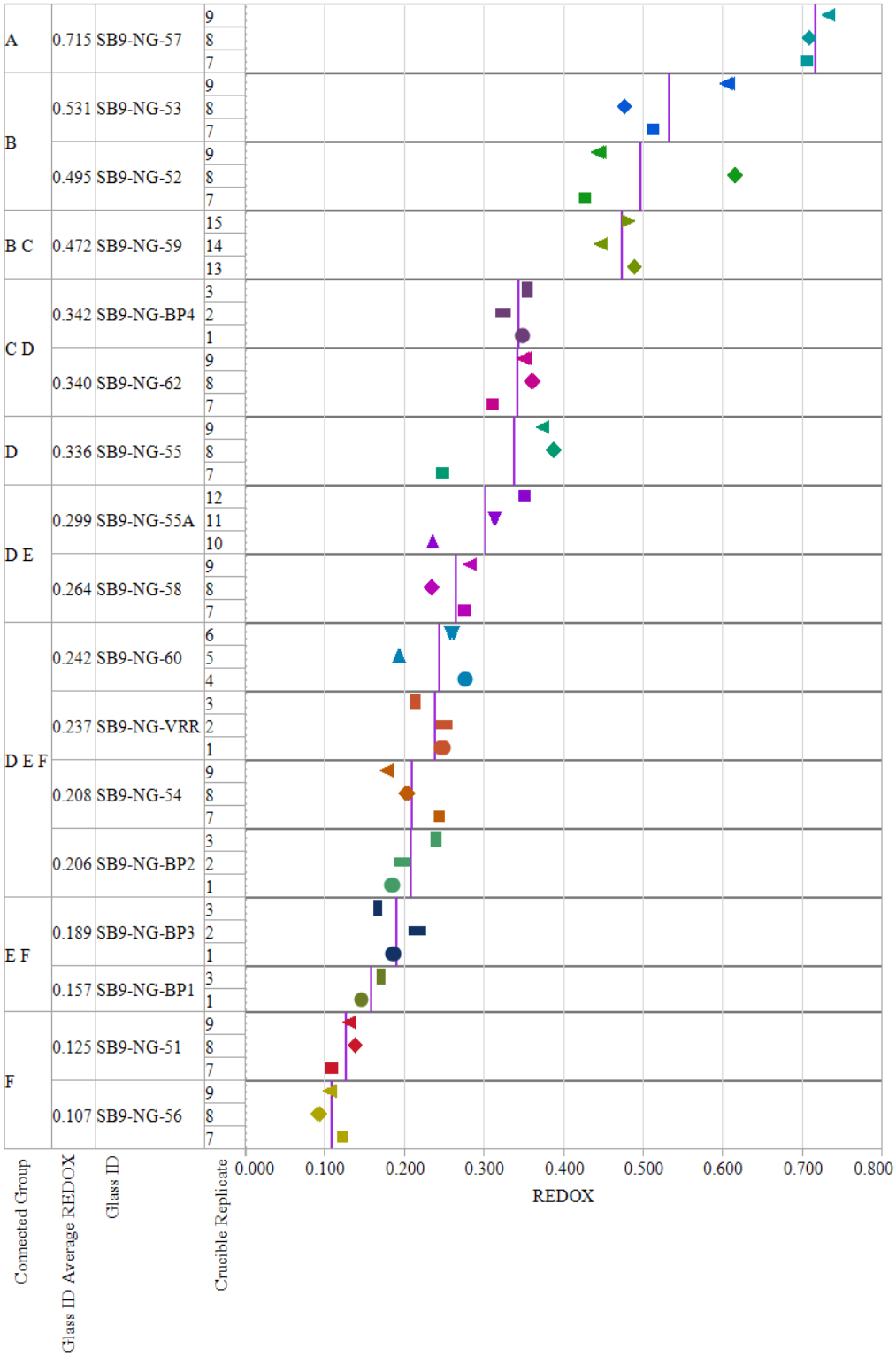

Figure 3-5. Statistical groupings of the REDOX measurements.

Note: The purple vertical line segments represent the average REDOX values for the study glasses. These average values are also part of the descriptive information provided in the plot.

3.4 Validation of Interim NG REDOX Model with All of the Improved NG REDOX Data

The historic NF REDOX database is given in Appendix A. The historic database consists of 139 data points and if the antifoam data from Reference 31 is included the database is 182 data points. For the 139 data point fit to Equation 21 the adjusted R^2 is 0.81 with a RMSE of 0.0704 while the 182 data point fit to Equation 21 has an adjusted R^2 of 0.83 and a RMSE of 0.0664 (Figure 3-6). The 182 point fit is preferred for comparison to the NG REDOX data because it has the antifoam data which goes up to $Fe^{2+}/\Sigma Fe$ values of 0.575.

The pilot scale and full scale DWPF validation data for the NF REDOX model is given in Appendix B. The NG REDOX database of CC_{hot} data is given in Appendix C. Note that Appendix C is only the NG REDOX data gathered since the interim NG REDOX model was developed, i.e. the data generated once the procedure was augmented with a way to calculate the viscosity of the crucible SRAT/frit mixture. This is the data given in Appendix C. Data that are shaded in Appendix C are measured $Fe^{2+}/\Sigma Fe$ that are considered outliers not suitable for REDOX modeling. During REDOX testing and measurement [44] triplicate experiments and triplicate analyses are performed so that outlier data can be eliminated and model error minimized. This methodology has been applied to all REDOX modeling since 1997 [19, 24, 25, 30, 31].

The NG REDOX data in Appendix C were modeled using the interim NG REDOX model (Equation 21). This improved NG data were overlain on the historic and antifoam NF REDOX data and are shown in Figure 3-6. The NG REDOX data generated with the improvements made to the CC_{hot} crucible methodology fit reasonably well to the historic REDOX data except for the samples circled and identified as feeds with low wt% solids in Figure 3-6. The adjusted R^2 and RMSE in Figure 3-6 is for the fit of the historic data.

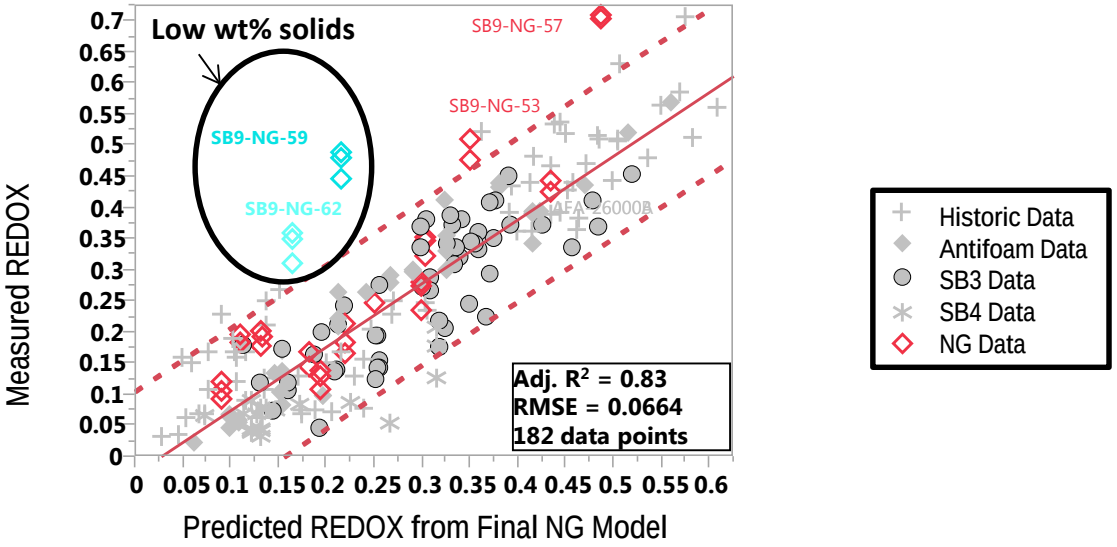

Figure 3-6. Comparison of the Improved NG REDOX Data Overlain on the Historic and antifoam (182 point) REDOX data plot.

No NG data are fit in this plot. Gray symbols are the Historic and antifoam data. The open diamonds are the Improved NG REDOX Data developed since the Interim REDOX Model was Developed.

3.5 Lack of Linearity in the 45/T Assumption and Impacts on the Large EE of Glycolate

The disparate improved NG REDOX data were examined in light of the normalization using 45/T to correct the concentrations in the feeds to a consistent weight percent solids so that the impacts of more dilute versus more concentrated feeds does not impact REDOX modeling [19, 24, 25, 30, 31]. To facilitate this comparison the calculated SME or total solids was plotted against the 45/T ratio assumption as shown in Figure 3-7. Below about 32 wt% solids 45/T assumption becomes non-linear.

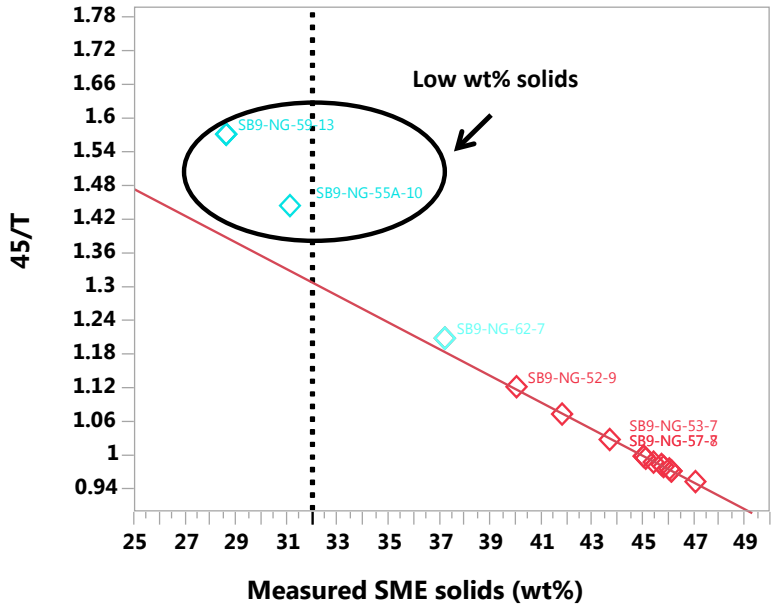

Figure 3-7. Non-linearity of the 45/T assumption in REDOX modeling below 32wt% solids.

While the DWPF has operated primarily in the >40 wt% SME solids region, crucible testing with the NF flowsheet has been as low as 35 wt% SME solids as shown in Figure 3-8. For the NF flowsheet a low SME wt% solids in Equation 21 is not impacted by the non-linearity in the 45/T assumption because the EE's of the reductants is in the 2-4 range although the oxidants can have EE's as high as five. With the NG flowsheet the glycolate has an EE of six and the non-linearity of the 45/T assumption in the low weight percent solids region causes larger errors in the NG REDOX prediction. Since 32% total solids, which includes the frit contribution, is close to the DWPF insoluble solids and yield stress design bases [50], it is recommended that a DWPF facility limit be imposed during implementation of the NG REDOX model (Equation 21).

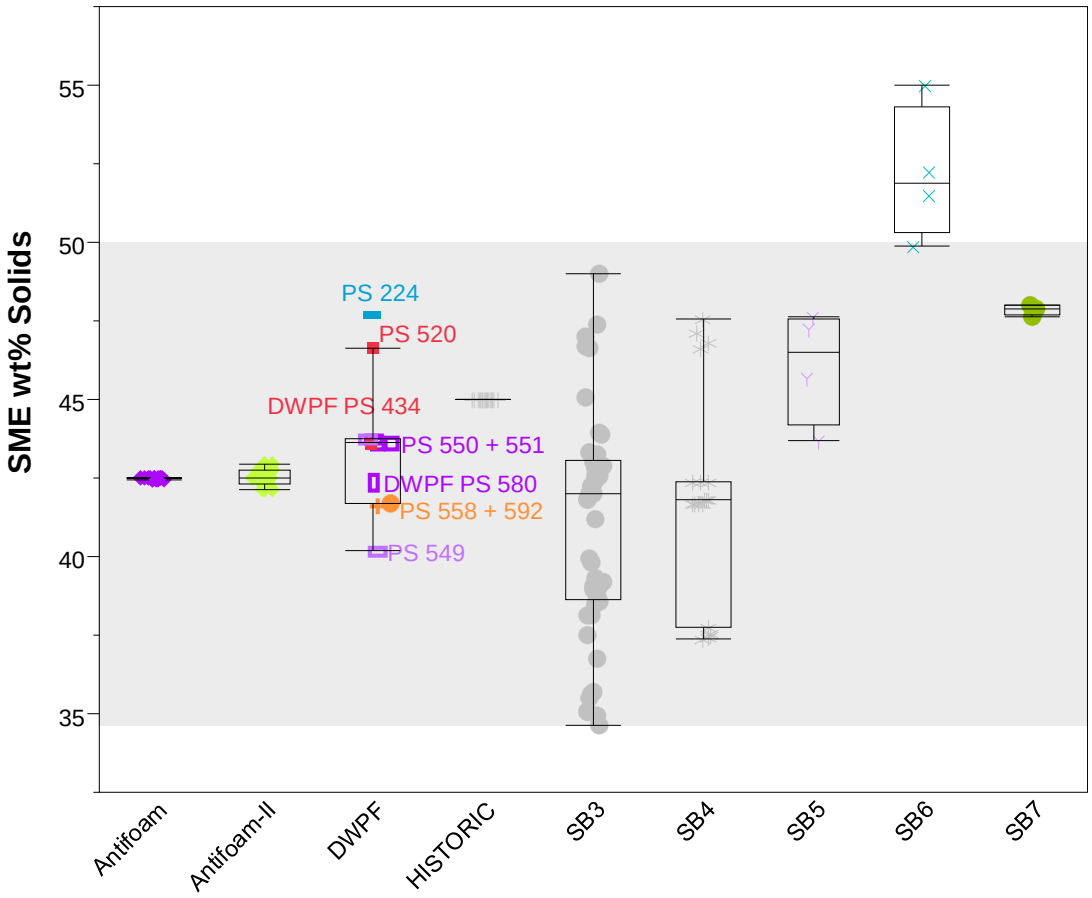

Figure 3-8. Ranges of SME wt% Solids Tested in Crucibles and Run in DWPF.

Shading indicates the modeling range of SME wt% solids tested.

3.6 Validation of Interim NG REDOX Model with a Subset of the Improved NG REDOX Data

When the two low wt% SME solids samples are excluded from the comparison of the NG REDOX data given in Appendix C to the NG interim REDOX model discussed in Section 1.8, it is seen in Figure 3-9a that only two data points fall outside the 95% confidence bands of the NG Interim model (Equation 21), SB9-NG-53 and SB9-NG-57. Both of these feeds contained a very high percent of glycolic acid (PRA>62%) (Figure 2-1). It is likely that some Fe^{2+} may have been created in the feed at these high values of PRA and Fe^{2+} in the SRAT/SME feed is not accounted for in any of the DWPF REDOX models. Moreover, SB9-NG-53 and SB9-NG-57 have measured $Fe^{2+}/\Sigma Fe$ that are outside the DWPF REDOX processing range of 0.09-0.33. At $Fe^{2+}/\Sigma Fe$ values >0.33 there can also be inherent difficulty in measurement due to the precipitation of secondary phases created by the reducing glass. Therefore, the adequacy of the interim REDOX model as the final NG REDOX model is evaluated both with and without the SB9-NG-53 and SB9-NG-57 data points.

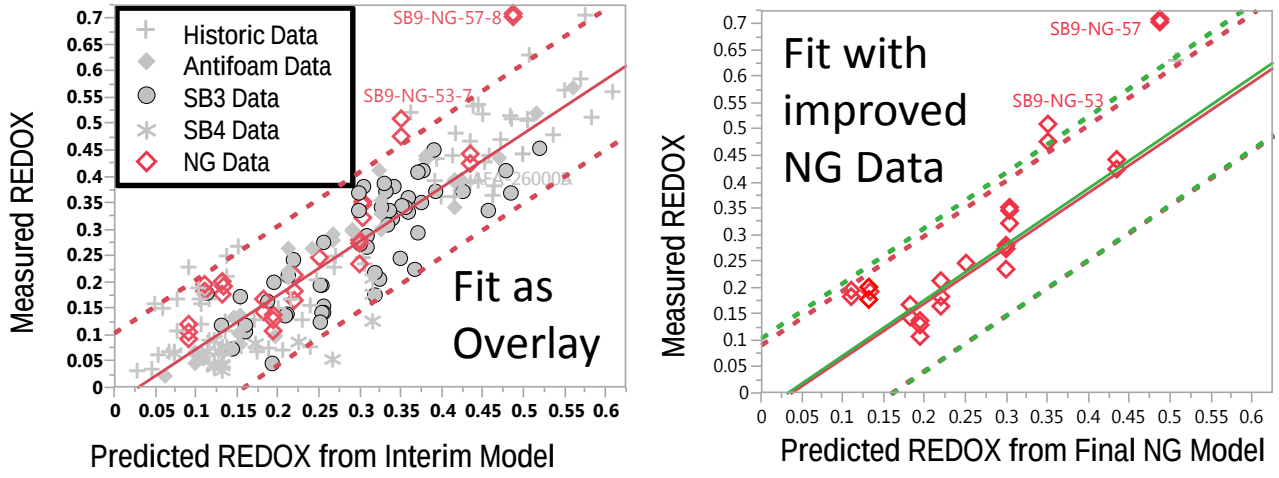

(a) (b)

Figure 3-9. Fitting the improved NG data as (a) an overlay or (b) as model data gives about the same slope and intercept.

The 95% confidence bands (red for model fit with SB9-NG-53 and SB9-NG-57 and green for model fit without SB9-NG-53 and SB9-NG-57) are slightly wider indicating a slightly poorer fit when the improved NG data are used in the modeling (Figure b).

Figure 3-9b demonstrates what would happen if Equation 21 were refit using the improved NG data including SB9-NG-53 and SB9-NG-57. The slope and intercept of the fit are the same but the error bands, and hence the model accuracy, would be a little lower than that given by Equation 21. For example, the 182 data points used to fit the data in Figure 3-9a and b give an adjusted R^2 of 0.83 and a RMSE of 0.0664 while the alternate 210 data points (NF, antifoam, and NG) used to fit the data in Figure 3-9b which gives an adjusted R^2 of 0.81 and a RMSE of 0.070. In either case, Figure 3-9a or b, the interim NG REDOX model can be used as the final NG REDOX model for the glycolate flowsheet.

Lastly, if one examines the balance of reductants versus oxidizers for the NG flowsheet compared to the NF flowsheet by comparing Figure 3-10 to Figure 1-2 one can see that the improved NG REDOX data fall on the 1:1 line but are in a much different region of oxidizers and reductants than the NF REDOX data. This is the utility of having a first principles EE transfer model to balance the reduction-oxidation equilibria.

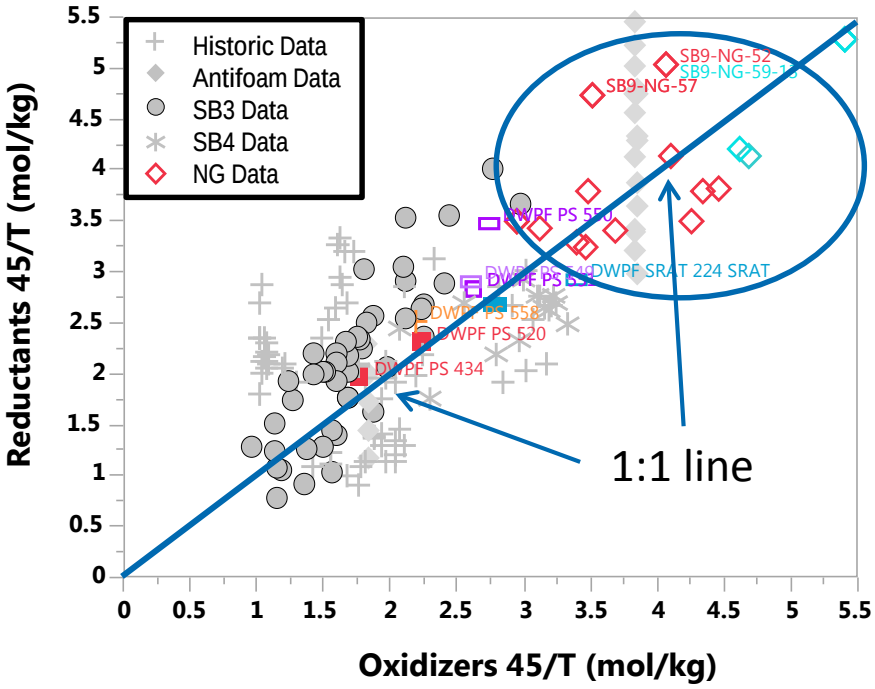

Figure 3-10. Reductants vs. Oxidants showing the balance (equilibrium) regions for the NF and NG flowsheets.

The NF and NG flowsheets are on the same 1:1 correlation due to the weighting of the various reductants and oxidants in Equation 21. Note that the solid diamonds are the antifoam REDOX data where the oxidants were not varied but the one reductant (antifoam) was varied. The open diamonds are the NG REDOX data presented in this study. The blue open diamonds are the NG REDOX data with low wt% solids (<32 wt% SME solids). The solid squares and open rectangles are DWPF PS samples.

3.7 Validation of Interim/Final NG REDOX Model with Pilot-Scale and Full-Scale DWPF Data

Because the Interim/Final NG REDOX model is based on the same balance between the oxidizers and reductants in the melter as the NF REDOX model, the pilot-scale and full-scale DWPF validation data from the NF flowsheet can be used as scale-up validation. The slurry melt rate furnace (SMRF), mini-melter (MM), and DWPF MFT and PS sample data are shown overlain on the Interim/Final NG REDOX model along with the historic, antifoam, and NG data in Figure 3-11. The comparison of the DWPF PS data is from non-bubbled operations to avoid the confusion of having to correct for Ar bubbling in the REDOX equation. Scale-up validation from the NF flowsheet is, therefore, applicable to the NG REDOX model.

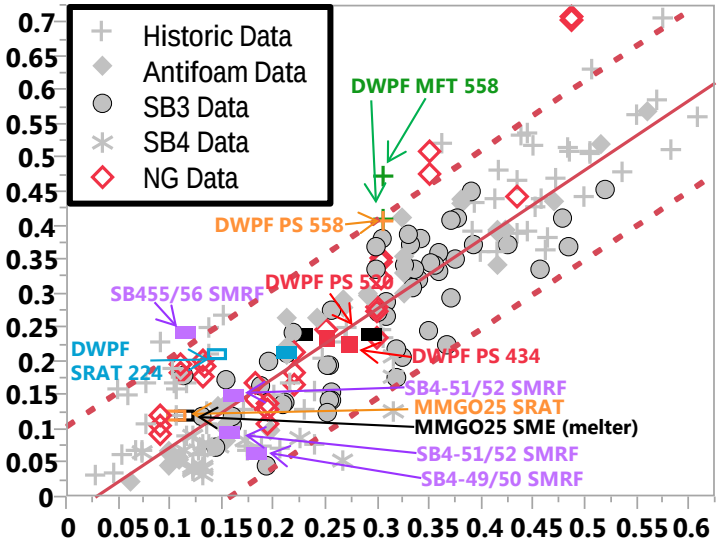

Figure 3-11. The Historic and antifoam (182 point) REDOX Data Plot with the Improved NG REDOX Data and the Slurry Melt Rate Furnace (SMRF), Mini-melter (MM), and DWPF Pour Spout (PS) Data Overlain.

4.0 Conclusions

The improved NG REDOX data have shown that the interim NG REDOX model can be used as the final NG REDOX model with a glycol EE of 6 and Mn EE=0 as shown in Equation 21 and given below:

$$\xi_{\text{A-gly}} = \left[\left(2[F] + 4[C] + 4[\text{O}_\text{T}] + 3.39 * eff\,[C_A] + 6[Gly] - 5[N] - 0[Mn] \right) \frac{45}{T} \right]$$

where
- [F] = formate (mol/kg feed)
- [C] = coal (carbon) (mol/kg feed)
- $[\text{O}_\text{T}]$ = $\text{oxalate}_{\text{Total}}$ (soluble and insoluble) (mol/kg feed)
- $[C_A]$ = carbon from antifoam (mol/kg feed)
- eff = effective antifoam impact = 0.85
- [gly] = glycolate (mol/kg feed)
- [N] = nitrate + nitrite (mol/kg feed)
- [Mn] = manganese (mol/kg feed)
- T = total solids (wt%)
- $\xi_{\text{A-gly}}$ = EE term with antifoam and glycolate

and

$$\frac{Fe^{2+}}{\Sigma Fe} = 0.2358 + 0.1999\xi_{A-gly}$$

The NG REDOX model given above can be used with or without the 0.1 offset term for Ar bubbling.

However, the NG REDOX model should not be used at SME weight percent solids below 32wt%.

Scale-up validation from the NF flowsheet is, therefore, applicable to the NG REDOX model.

This study demonstrates the following:

- the final NG REDOX model and the interim NG REDOX model are the same
- the final NG REDOX model cannot be used on feeds less than 32wt% SME solids unless a mathematical algorithm is developed for feeds with <32wt% SME solids
- the final NG REDOX model has an Mn EE term of 0 in the range of acid stoichiometries examined in this study (76.9 to 123.2% KMA basis or 80-129% on the Hsu basis): lower concentrations of glycolic acid in the presence of higher nitric acid would need to be investigated to determine if the Mn EE=0 is still valid

This study recommends the following:

- Since 32% total solids, which includes the frit contribution, is close to the DWPF insoluble solids and yield stress design bases, it is recommended that a DWPF facility limit be imposed during implementation of the NG REDOX model.
- PS samples be taken to confirm the NG REDOX model as was done with the NF REDOX model
- the linearity of the Ar term during processing with the NG flowsheet be checked with data from the pour spout samples

APPENDIX A. Historic REDOX Database for NF Flowsheet

Table A1. NF REDOX DATABASE (CC_{hot})

Sample ID	Frit	SRAT/SME(MFT)	Target Waste Loading	SRAT pH	Measured REDOX	Fe^{+2} (units of absorbance)	# Fe Measurements	Total Fe (units of absorbnce)	SME wt% solids	Formate (mol/kg)	Nitrate (mol/kg)	Oxalate (mol/kg)	Coal (mol/kg)	Mn (mol/kg)	Antifoam (mol/kg)
HISTORIC REDOX MODEL DATA (FROM TABLE I IN 19)															
S9-L-F300	200	SME			0.566		1		45	1.559	0.239	0.000	0.000	0.091	0.033
S9-L-F800	200	SME			0.587		1		45	1.587	0.229	0.000	0.000	0.091	0.033
S9-L-F800	200	SME			0.514		1		45	1.630	0.233	0.000	0.000	0.091	0.033
S9-L-N1000	200	SME			0.157		1		45	1.468	0.512	0.000	0.000	0.091	0.033
S9-L-N1000	200	SME			0.204		1		45	1.381	0.469	0.000	0.000	0.091	0.033
S9-L-N50	200	SME			0.511		1		45	1.394	0.236	0.000	0.000	0.091	0.033
S9-L-N50	200	SME			0.536		1		45	1.222	0.215	0.000	0.000	0.091	0.033
S9-L-N500	200	SME			0.361		1		45	1.522	0.373	0.000	0.000	0.091	0.033
S9-L-N500	200	SME			0.393		1		45	1.387	0.328	0.000	0.000	0.091	0.033
S9-L-P1500	200	SME			0.479		1		45	1.562	0.253	0.000	0.000	0.091	0.033
S9-L-P1500	200	SME			0.511		1		45	1.428	0.232	0.000	0.000	0.091	0.033
S9-L-P3000	200	SME			0.522		1		45	0.913	0.167	0.000	0.000	0.091	0.033
S9-L-P3000	200	SME			0.482		1		45	1.139	0.203	0.000	0.000	0.091	0.033
S9-L-P200	200	SME			0.519		1		45	1.279	0.226	0.000	0.000	0.091	0.033
S9-L-P200	200	SME			0.538		1		45	1.307	0.242	0.000	0.000	0.091	0.033
S10-L-F1500	168	SME			0.563		1		45	1.397	0.096	0.000	0.000	0.109	0.033
S10-L-F1500	168	SME			0.707		1		45	1.307	0.094	0.000	0.000	0.109	0.033
S10-L-F300	168	SME			0.516		1		45	1.108	0.105	0.000	0.000	0.109	0.033
S10-L-F300	168	SME			0.471		1		45	1.070	0.103	0.000	0.000	0.109	0.033
S10-L-F800	168	SME			0.509		1		45	1.131	0.094	0.000	0.000	0.109	0.033
S10-L-F800	168	SME			0.63		1		45	1.139	0.094	0.000	0.000	0.109	0.033
S10-L-N100	168	SME			0.442		1		45	0.990	0.128	0.000	0.000	0.109	0.033
S10-L-N100	168	SME			0.364		1		45	1.006	0.133	0.000	0.000	0.109	0.033

Sample ID	Frit	SRAT/SME(MFT)	Target Waste Loading	SRAT pH	Measured REDOX	Fe^{+2} (units of absorbance)	# Fe Measurements	Total Fe (units of absorbnce)	SME wt% solids	Formate (mol/kg)	Nitrate (mol/kg)	Oxalate (mol/kg)	Coal (mol/kg)	Mn (mol/kg)	Antifoam (mol/kg)
S10-L-N1000	168	SME			0.129		1		45	1.052	0.339	0.000	0.000	0.109	0.033
S10-L-N1000	168	SME			0.152		1		45	0.954	0.328	0.000	0.000	0.109	0.033
S10-L-N500	168	SME			0.237		1		45	1.003	0.241	0.000	0.000	0.109	0.033
S10-L-N500	168	SME			0.249		1		45	0.998	0.242	0.000	0.000	0.109	0.033
S10-L-P200	168	SME			0.393		1		45	1.013	0.106	0.000	0.000	0.109	0.033
S10-L-P200	168	SME			0.384		1		45	1.059	0.107	0.000	0.000	0.109	0.033
S10-L-N50	168	SME			0.434		1		45	0.856	0.095	0.000	0.000	0.109	0.033
S10-L-P1500	168	SME			0.441		1		45	1.023	0.097	0.000	0.000	0.109	0.033
S10-L-P1500	168	SME			0.365		1		45	1.039	0.100	0.000	0.000	0.109	0.033
S10-L-P3000	168	SME			0.445		1		45	1.135	0.101	0.000	0.000	0.109	0.033
S10-L-P3000	168	SME			0.468		1		45	0.967	0.098	0.000	0.000	0.109	0.033
S10-L-P500	168	SME			0.391		1		45	0.983	0.105	0.000	0.000	0.109	0.033
S10-L-P500	168	SME			0.429		1		45	1.019	0.103	0.000	0.000	0.109	0.033
I-L-P1500	202	SME			0.033		1		45	1.011	0.549	0.000	0.000	0.084	0.033
I-L-P200	202	SME			0.035		1		45	0.975	0.517	0.000	0.000	0.084	0.033
I-L-P3000	202	SME			0.063		1		45	0.911	0.482	0.000	0.000	0.084	0.033
I-L-PF1500	202	SME			0.077		1		45	1.289	0.499	0.000	0.000	0.084	0.033
I-L-PF1500	202	SME			0.131		1		45	1.342	0.537	0.000	0.000	0.084	0.033
I-L-PF5/8	202	SME			0.063		1		45	1.291	0.555	0.000	0.000	0.084	0.033
I-L-PF5/8	202	SME			0.126		1		45	1.227	0.527	0.000	0.000	0.084	0.033
26-1000	202	SME			0.071		1		45	0.833	0.292	0.000	0.000	0.091	0.033
27-250	202	SME			0.07		1		45	0.406	0.260	0.000	0.000	0.091	0.033
27-750	202	SME			0.068		1		45	0.571	0.219	0.000	0.000	0.091	0.033
27-750	202	SME			0.077		1		45	0.502	0.191	0.000	0.000	0.091	0.033
DWPF-Batch1-9	202	SME			0.25		1		45	1.016	0.302	0.000	0.000	0.089	0.033
DWPF-Batch1-9	202	SME			0.08		1		45	0.935	0.302	0.000	0.000	0.089	0.033
DWPF-Batch1-10	202	SME			0.23		1		45	0.935	0.272	0.000	0.000	0.089	0.033
DWPF-Batch1-10	202	SME			0.17		1		45	0.913	0.317	0.000	0.000	0.089	0.033
DWPF-Batch1-11	202	SME			0.23		1		45	0.545	0.295	0.000	0.000	0.089	0.033

Sample ID	Frit	SRAT/SME(MFT)	Target Waste Loading	SRAT pH	Measured REDOX	Fe^{+2} (units of absorbance)	# Fe Measurements	Total Fe (units of absorbnce)	SME wt% solids	Formate (mol/kg)	Nitrate (mol/kg)	Oxalate (mol/kg)	Coal (mol/kg)	Mn (mol/kg)	Antifoam (mol/kg)
DWPF-Batch1-11	202	SME			0.16		1		45	0.501	0.317	0.000	0.000	0.089	0.033
DWPF-Batch1-12	202	SME			0.17		1		45	0.530	0.302	0.000	0.000	0.089	0.033
DWPF-Batch1-12	202	SME			0.15		1		45	0.523	0.317	0.000	0.000	0.089	0.033
DWPF-Batch1-13	202	SME			0.21		1		45	0.663	0.295	0.000	0.000	0.089	0.033
DWPF-Batch1-13	202	SME			0.09		1		45	0.685	0.324	0.000	0.000	0.089	0.033
DWPF-Batch1-14	202	SME			0.25		1		45	0.648	0.287	0.000	0.000	0.089	0.033
DWPF-Batch1-14	202	SME			0.17		1		45	0.611	0.295	0.000	0.000	0.089	0.033
DWPF-Batch1-15	202	SME			0.11		1		45	0.641	0.287	0.000	0.000	0.089	0.033
DWPF-Batch1-15	202	SME			0.19		1		45	0.633	0.317	0.000	0.000	0.089	0.033
DWPF-Batch1-22	202	SME			0.07		1		45	0.560	0.317	0.000	0.000	0.089	0.033
DWPF-Batch1-16	202	SME			0.27		1		45	0.515	0.221	0.000	0.000	0.089	0.033
DWPF-Batch1-16	202	SME			0.12		1		45	0.457	0.243	0.000	0.000	0.089	0.033
DWPF-Batch1-21	202	SME			0.16		1		45	0.530	0.272	0.000	0.000	0.089	0.033
DWPF-Batch1-21	202	SME			0.11		1		45	0.604	0.331	0.000	0.000	0.089	0.033
DWPF-Batch1-22	202	SME			0.17		1		45	0.508	0.265	0.000	0.000	0.089	0.033
SB3 REDOX MODEL DATA (FROM TABLE V IN REFERENCE 24)															
SB3-1-25-320A	320	SRAT	25	.	0.12	0.049	4	0.407	42.8	0.338	0.162	0.000	0.000	0.069	0.033
SB3-1-30-320A	320	SRAT	30	.	0.07	0.029	4	0.393	38.75	0.399	0.191	0.000	0.000	0.081	0.033
SB3-5-30-320A	320	SRAT	30	.	0.41	0.176	4	0.433	45.09	0.387	0.188	0.264	0.000	0.061	0.033
SB3-5-35-320A	320	SRAT	35	.	0.45	0.223	4	0.494	41.78	0.443	0.216	0.302	0.000	0.069	0.033
SB3-6-25-320A	320	SRAT	25	.	0.37	0.131	4	0.353	46.66	0.347	0.134	0.124	0.000	0.058	0.033
SB3-6-30-320A	320	SRAT	30	.	0.27	0.104	4	0.390	42.58	0.409	0.158	0.146	0.000	0.069	0.033
SB3-7-25-320A	320	SRAT	25	.	0.12	0.042	4	0.337	42.01	0.325	0.284	0.254	0.000	0.053	0.033
SB3-7-30-320A	320	SRAT	30	.	0.19	0.075	4	0.387	38.15	0.382	0.334	0.298	0.000	0.062	0.033
SB3-7-35-320A	320	SRAT	35	.	0.14	0.061	4	0.427	35.07	0.436	0.381	0.341	0.000	0.070	0.033
SB3-15-30-320A	320	SRAT	30	.	0.33	0.129	4	0.390	39.04	0.660	0.285	0.228	0.007	0.065	0.033
SB3-1-25-202A	202	SRAT	25	.	0.10	0.028	4	0.263	42.84	0.337	0.162	0.000	0.000	0.069	0.033
SB3-1-35-202A	202	SRAT	35	.	0.12	0.032	4	0.267	35.5	0.459	0.220	0.000	0.000	0.093	0.033

Sample ID	Frit	SRAT/SME(MFT)	Target Waste Loading	SRAT pH	Measured REDOX	Fe^{+2} (units of absorbance)	# Fe Measurements	Total Fe (units of absorbnce)	SME wt% solids	Formate (mol/kg)	Nitrate (mol/kg)	Oxalate (mol/kg)	Coal (mol/kg)	Mn (mol/kg)	Antifoam (mol/kg)
SB3-2-25-200A	200	SRAT	25	.	0.24	0.101	4	0.415	42.99	0.321	0.167	0.000	0.082	0.064	0.033
SB3-2-30-200A	200	SRAT	30	.	0.21	0.083	4	0.389	38.91	0.380	0.198	0.000	0.097	0.076	0.033
SB3-2-35-200A	200	SRAT	35	.	0.14	0.053	4	0.391	35.65	0.437	0.227	0.000	0.111	0.087	0.033
SB3-3-25-200A	200	SRAT	25	.	0.28	0.128	4	0.463	43.85	0.409	0.166	0.000	0.080	0.060	0.033
SB3-4-25-202A	202	SRAT	25	.	0.14	0.048	4	0.349	43.24	0.314	0.170	0.000	0.082	0.066	0.033
SB3-6-25-202A	202	SRAT	25	.	0.34	0.102	4	0.304	46.67	0.347	0.134	0.124	0.000	0.058	0.033
SB3-6-30-202A	202	SRAT	30	.	0.29	0.112	4	0.388	42.58	0.409	0.158	0.146	0.000	0.069	0.033
SB3-7-25-202A	202	SRAT	25	.	0.19	0.093	4	0.483	42.01	0.325	0.284	0.254	0.000	0.053	0.033
SB3-7-30-202A	202	SRAT	30	.	0.14	0.062	4	0.439	38.15	0.382	0.334	0.298	0.000	0.062	0.033
SB3-7-35-202A	202	SRAT	35	.	0.16	0.058	4	0.370	35.07	0.436	0.381	0.341	0.000	0.070	0.033
SB3-8-25-202A	202	SRAT	25	.	0.27	0.097	4	0.357	41.79	0.322	0.286	0.252	0.064	0.051	0.033
SB3-8-35-202A	202	SRAT	35	.	0.18	0.087	4	0.493	34.91	0.430	0.383	0.337	0.085	0.069	0.033
SB3-9-25-202A	202	SRAT	25	.	0.24	0.096	4	0.395	42.89	0.343	0.230	0.239	0.062	0.054	0.033
SB3-9-30-202A	202	SRAT	30	.	0.22	0.089	4	0.396	39.02	0.403	0.270	0.280	0.072	0.063	0.033
SB3-10-35-202A	202	SRAT	35	.	0.34	0.139	4	0.407	35.71	0.519	0.286	0.262	0.008	0.070	0.033
SB3-11-25-202A	202	SRAT	25	.	0.39	0.122	4	0.315	42.79	0.430	0.199	0.189	0.006	0.054	0.033
SB3-12-25-202A	202	SRAT	25	.	0.33	0.116	4	0.346	43.03	0.443	0.248	0.194	0.062	0.053	0.033
SB3-12-30-202A	202	SRAT	30	.	0.35	0.144	4	0.415	39.21	0.519	0.290	0.227	0.072	0.063	0.033
SB3-13-25-202A	202	SRAT	25	.	0.34	0.108	4	0.316	43.15	0.507	0.264	0.210	0.062	0.055	0.033
SB3-13-30-202A	202	SRAT	30	.	0.35	0.129	4	0.366	39.31	0.594	0.310	0.247	0.073	0.065	0.033
SB3-14-30-202A	202	SRAT	30	.	0.37	0.142	4	0.383	39.01	0.508	0.272	0.253	0.008	0.064	0.033
SB3-15-25-202A	202	SRAT	25	.	0.38	0.125	4	0.326	42.87	0.564	0.244	0.194	0.006	0.056	0.033
SB3-15-30-202A	202	SRAT	30	.	0.36	0.169	4	0.469	39.04	0.661	0.285	0.228	0.007	0.065	0.033
SB3-16-25-202A	202	SRAT	25	.	0.32	0.119	4	0.371	42.52	0.436	0.264	0.225	0.062	0.056	0.033
SB3-18-25-202A	202	SRAT	25	.	0.04	0.017	4	0.384	43.32	0.430	0.230	0.000	0.081	0.068	0.033
SB3-22-30-320	320	SME	30	.	0.41	0.176	4	0.430	49	1.077	0.594	0.282	0.077	0.000	0.033
SB3-23-30-320	320	SME	30	.	0.22	0.110	4	0.502	47.4	0.730	0.446	0.187	0.087	0.000	0.033
SB3-24-25-202	202	SRAT	25	.	0.41	0.113	4	0.275	42.32	0.263	0.326	0.533	0.066	0.035	0.033
SB3-24-30-202	202	SRAT	30	.	0.45	0.127	4	0.281	38.54	0.308	0.382	0.623	0.078	0.041	0.033

Sample ID	Frit	SRAT/SME(MFT)	Target Waste Loading	SRAT pH	Measured REDOX	Fe^{+2} (units of absorbance)	# Fe Measurements	Total Fe (units of absorbnce)	SME wt% solids	Formate (mol/kg)	Nitrate (mol/kg)	Oxalate (mol/kg)	Coal (mol/kg)	Mn (mol/kg)	Antifoam (mol/kg)
SB3-A1-25-202	202	SRAT	25	.	0.37	0.126	4	0.339	41.19	0.540	0.346	0.402	0.063	0.072	0.033
SB3-A1-30-202	202	SRAT	30	.	0.34	0.110	4	0.327	37.53	0.630	0.403	0.468	0.074	0.084	0.033
SB3-A1-35-202	202	SRAT	35	.	0.37	0.177	4	0.477	34.63	0.714	0.457	0.531	0.084	0.095	0.033
SB3-A2-25-202	202	SRAT	25	.	0.38	0.132	4	0.346	46.69	0.399	0.232	0.193	0.069	0.087	0.033
SB3-A2-30-202	202	SRAT	30	.	0.21	0.083	4	0.399	39.79	0.528	0.307	0.256	0.091	0.115	0.033
SB3-A2-35-202	202	SRAT	35	.	0.31	0.125	4	0.404	36.73	0.602	0.350	0.291	0.104	0.131	0.033
SB3-A3-25-202	202	SRAT	25	.	0.29	0.056	4	0.192	42.24	0.539	0.280	0.254	0.075	0.083	0.033
SB3-A3-30-202	202	SRAT	30	.	0.37	0.124	4	0.335	38.52	0.629	0.327	0.296	0.088	0.097	0.033
SB3-A4-25-202	202	SRAT	25	.	0.20	0.102	4	0.509	43.92	0.440	0.207	0.005	0.098	0.111	0.033
SB3-A4-30-202	202	SRAT	30	.	0.16	0.099	4	0.608	39.94	0.518	0.243	0.006	0.116	0.131	0.033
MM Feed 200 SME (crucible)	200	SME	25.5	.	0.17	0.068	4	0.394	47	0.844	0.346	0.000	0.000	0.091	0.033
MM Feed 320 SME (crucible)	320	SME	25.5	.	0.18	0.064	4	0.360	47	0.770	0.333	0.000	0.000	0.115	0.033
SB4 REDOX MODEL DATA (FROM TABLE 5 IN REFERENCE 30)															
SB4-20-418 (coppt)	418		35		0.07	0.032	4	0.468	37.78	1.002	0.454	0.000	0.000	0.104	0.033
SB4RE-32-418-35	418	SRAT	35	9.37	0.04	0.026	4	0.622	42.39	0.784	0.305	0.000	0.000	0.126	0.033
SB4RE-32-503-35	503	SRAT	35	9.37	0.03	0.020	4	0.607	42.39	0.784	0.305	0.000	0.000	0.126	0.033
SB4RE-32-P2-2-35	p2-2	SRAT	35	9.37	0.05	0.036	4	0.783	42.39	0.784	0.305	0.000	0.000	0.126	0.033
SB4RE-34-FA only	418	SRAT	35	.	0.18	0.117	4	0.657	41.79	1.092	0.27	0.000	0.000	0.113	0.033
SB4RE-34-FA only	503	SRAT	35	.	0.21	0.177	4	0.850	41.79	1.092	0.27	0.000	0.000	0.113	0.033
SB4RE-34-FA only	p2-2	SRAT	35	.	0.13	0.107	4	0.842	41.79	1.092	0.27	0.000	0.000	0.113	0.033
SB4-41-418	418	SRAT	35	7.88	0.05	0.035	4	0.760	41.66	0.975	0.404	0.000	0.000	0.11	0.033
SB4-41-P2-2	P2-2	SRAT	35	7.88	0.04	0.040	4	0.930	41.66	0.975	0.404	0.000	0.000	0.11	0.033
SB4-41-418 full formic (50 gal)	418	SRAT	35	7.88	0.09	0.055	4	0.603	41.66	0.975	0.404	0.000	0.000	0.11	0.033
SB4-41-418 half formic (25 gal)	418	SRAT	35	7.88	0.04	0.020	4	0.505	41.66	0.975	0.404	0.000	0.000	0.11	0.033
SB4-49	418	SRAT	35	.	0.08	0.063	8	0.801	37.38	1.074	0.408	0.000	0.000	0.128	0.033
SB4-51	425	SRAT	35	.	0.07	0.067	4	0.966	37.56	1.051	0.402	0.000	0.000	0.128	0.033

Sample ID	Frit	SRAT/SME(MFT)	Target Waste Loading	SRAT pH	Measured REDOX	Fe^{+2} (units of absorbance)	# Fe Measurements	Total Fe (units of absorbnce)	SME wt% solids	Formate (mol/kg)	Nitrate (mol/kg)	Oxalate (mol/kg)	Coal (mol/kg)	Mn (mol/kg)	Antifoam (mol/kg)
SB4-49/50 MIX	418	SRAT	35	.	0.08	0.063	8	0.801	37.53	1.059	0.396	0.000	0.000	0.129	0.033
SB4-51/52 MIX	425	SRAT	35	.	0.07	0.067	4	0.966	37.43	0.93	0.368	0.000	0.000	0.125	0.033
SB4-61	503	SRAT	35	8.17	0.06	0.051	4	0.913	46.65	1.351	0.383	0.000	0.000	0.145	0.033
SB4-62	503	SRAT	35	6.83	0.08	0.065	4	0.860	47.57	1.415	0.54	0.000	0.000	0.139	0.033
SB4-63	503	SRAT	35	5.27	0.08	0.075	4	0.896	46.83	1.398	0.517	0.000	0.000	0.128	0.033
SB4-64	503	SRAT	35	4.78	0.09	0.079	2	0.894	47.13	1.490	0.498	0.000	0.000	0.129	0.033
ANTIFOAM REDOX MODEL DATA (TABLE 2 IN REFERENCE 31)															
AFA-10000A	418	SME	35.9		0.022	0.011	1	0.5	42.45	1.438	0.586	0.004	0	0.1392	0.369
AFA-10000B	418	SME	35.9		0.022	0.011	1	0.501	42.45	1.438	0.586	0.004	0	0.1392	0.369
AFA-12000A	418	SME	35.9		0.054	0.029	1	0.533	42.48	1.438	0.585	0.004	0	0.1392	0.446
AFA-12000B	418	SME	35.9		0.056	0.03	1	0.532	42.48	1.438	0.585	0.004	0	0.1392	0.446
AFA-14000A	418	SME	35.9		0.102	0.052	1	0.508	42.48	1.438	0.585	0.004	0	0.1392	0.515
AFA-14000B	418	SME	35.9		0.102	0.052	1	0.51	42.48	1.438	0.585	0.004	0	0.1392	0.515
AFA-16000A	418	SME	35.9		0.098	0.049	1	0.501	42.47	1.438	0.586	0.004	0	0.1392	0.592
AFA-16000B	418	SME	35.9		0.096	0.048	1	0.500	42.47	1.438	0.586	0.004	0	0.1392	0.592
AFA-18000A	418	SME	35.9		0.261	0.129	1	0.493	42.46	1.438	0.586	0.004	0	0.1392	0.666
AFA-18000B	418	SME	35.9		0.260	0.128	1	0.492	42.46	1.438	0.586	0.004	0	0.1392	0.666
AFA-20000A	418	SME	35.9		0.299	0.14	1	0.468	42.47	1.438	0.585	0.004	0	0.1392	0.745
AFA-20000B	418	SME	35.9		0.296	0.139	1	0.469	42.47	1.438	0.585	0.004	0	0.1392	0.745
AFA-22000A	418	SME	35.9		0.365	0.185	1	0.507	42.47	1.438	0.586	0.004	0	0.1392	0.814
AFA-22000B	418	SME	35.9		0.366	0.185	1	0.506	42.47	1.438	0.586	0.004	0	0.1392	0.814
AFA-24000A	418	SME	35.9		0.440	0.216	1	0.492	42.47	1.438	0.585	0.004	0	0.1392	0.891
AFA-24000B	418	SME	35.9		0.434	0.214	1	0.494	42.47	1.438	0.585	0.004	0	0.1392	0.891
AFA-26000A	418	SME	35.9		0.393	0.189	1	0.482	42.47	1.438	0.586	0.004	0	0.1392	0.962
AFA-26000B	418	SME	35.9		0.393	0.189	1	0.482	42.47	1.438	0.586	0.004	0	0.1392	0.962
AFA-28000A	418	SME	35.9		0.434	0.208	1	0.479	42.47	1.438	0.585	0.004	0	0.1392	1.038
AFA-28000B	418	SME	35.9		0.434	0.208	1	0.479	42.47	1.438	0.585	0.004	0	0.1392	1.038
AFA-30000A	418	SME	35.9		0.519	0.261	1	0.503	42.48	1.438	0.585	0.004	0	0.1392	1.112

Sample ID	Frit	SRAT/SME(MFT)	Target Waste Loading	SRAT pH	Measured REDOX	Fe^{+2} (units of absorbance)	# Fe Measurements	Total Fe (units of absorbnce)	SME wt% solids	Formate (mol/kg)	Nitrate (mol/kg)	Oxalate (mol/kg)	Coal (mol/kg)	Mn (mol/kg)	Antifoam (mol/kg)
AFA-30000B	418	SME	35.9		0.518	0.261	1	0.504	42.48	1.438	0.585	0.004	0	0.1392	1.112
AFA-32000A	418	SME	35.9		0.568	0.278	1	0.489	42.47	1.438	0.585	0.004	0	0.1392	1.184
AFA-32000B	418	SME	35.9		0.567	0.278	1	0.49	42.47	1.438	0.585	0.004	0	0.1392	1.184
AFA-13312A	418	SME	35.9		0.134	0.056	1	0.417	42.49	1.437	0.585	0.004	0	0.1391	0.507
AFA-21166A	418	SME	35.9		0.411	0.169	1	0.411	42.47	1.438	0.586	0.004	0	0.1392	0.799
AFA-25093A	418	SME	35.9		0.391	0.149	1	0.3815	42.47	1.438	0.586	0.004	0	0.1392	0.949
AFA-25093B	418	SME	35.9		0.342	0.1375	1	0.4025	42.48	1.438	0.585	0.004	0	0.1392	0.948
AFA-25093C	418	SME	35.9		0.394	0.15	1	0.3805	42.48	1.438	0.585	0.004	0	0.1392	0.948
FCJ-HG-800A	418	SME	35.9		0.065	0.033	1	0.504	42.91	0.836	0.268	0.0016	0	0.0834	800
FCJ-HG-800B	418	SME	35.9		0.046	0.023	1	0.497	42.91	0.836	0.268	0.0016	0	0.0834	800
FCJ-HG-800C	418	SME	35.9		0.063	0.031	1	0.49	42.91	0.836	0.268	0.0016	0	0.0834	800
FCJ-HG-3100A	418	SME	35.9		0.136	0.067	1	0.492	42.72	0.825	0.266	0.0019	0	0.0830	3100
FCJ-HG-3100B	418	SME	35.9		0.081	0.060	1	0.74	42.72	0.825	0.266	0.0019	0	0.0830	3100
FCJ-HG-3100C	418	SME	35.9		0.168	0.078	1	0.463	42.72	0.825	0.266	0.0019	0	0.0830	3100
FCJ-HG-5400A	418	SME	35.9		0.219	0.109	1	0.497	42.52	0.814	0.264	0.0022	0	0.0826	5400
FCJ-HG-5400B	418	SME	35.9		0.264	0.131	1	0.496	42.53	0.814	0.264	0.0022	0	0.0826	5400
FCJ-HG-5400C	418	SME	35.9		0.207	0.100	1	0.483	42.52	0.814	0.264	0.0022	0	0.0826	5400
FCJ-HG-7700A	418	SME	35.9		0.278	0.131	1	0.472	42.33	0.803	0.263	0.0025	0	0.0822	7700
FCJ-HG-7700B	418	SME	35.9		0.289	0.142	1	0.491	42.33	0.803	0.263	0.0025	0	0.0822	7700
FCJ-HG-10000A	418	SME	35.0		0.300	0.138	1	0.46	42.15	0.793	0.261	0.0028	0	0.0819	10000
FCJ-HG-10000B	418	SME	35.0		0.355	0.173	1	0.488	42.15	0.793	0.261	0.0028	0	0.0819	10000
FCJ-HG-10000C	418	SME	35.0		0.328	0.154	1	0.469	42.15	0.793	0.261	0.0028	0	0.0819	10000

APPENDIX B. Validation Database for NF Flowsheet

Table B1. NF REDOX DATABASE (Various Pilot Scale and Full Scale DWPF Testing)

Sample ID	Frit	SRAT/SME(MFT)	Target Waste Loading	SRAT pH	Measured REDOX	Fe^{+2} (units of absorbance)	# Fe Measurements	Total Fe (units of absorbance)	SME wt% solids	Formate (mol/kg)	Nitrate (mol/kg)	Oxalate (mol/kg)	Coal (mol/kg)	Mn (mol/kg)	Antifoam (mol/kg)
VALIDATION DATA (FROM TABLE IX IN REFERENCE 24) and SB4 SLURRY-FED MELT RATE FURNACE (SMRF) TESTING)															
MMGO25 SRAT	320	SRAT	25.5	.	0.12	0.120	4	1.000	41.39	0.393	0.215	0.000	0.000	0.093	0.033
MMGO25 SME	320	SME	25.5	.	0.12	0.120	4	1.000	47	0.770	0.333	0.000	0.000	0.115	0.033
SMRF 202 SME	202	SME			0.239	0.081		0.339	47.1	0.506	0.412	0.351	0.070	0.087	0.033
SMRF 202 SRAT	202	SRAT			0.239	0.081		0.339	47.1	0.521	0.468	0.348	0.070	0.100	0.033
SB4-49/50 SMRF	418	SRAT	35		0.064	0.064	4	1.000	44.15	1.734	0.633	0.000	0.000	0.131	0.033
SB4-51/52A SMRF	425	SRAT	35		0.094	0.094	4	1.000	44.40	1.575	0.599	0.000	0.000	0.127	0.033
SB4-51/52B SMRF	425	SRAT	35		0.149	0.149	4	1.000	44.30	1.577	0.596	0.000	0.000	0.127	0.033
SB4-5556 SMRF	503	SRAT	35	8.00	0.241	0.241	4	1.000	44.15	1.295	0.528	0.000	0.000	0.129	0.033
DWPF POUR SPOUT (PS) VALIDATION TESTING WITH AND WITHOUT ANTIFOAM															
DWPF SME 224	200	PS	35		0.21	0.21	6	1.000	47.70	1.291	0.506	0	0	0.055	0.033
DWPF SRAT 224	200	SRAT	35		0.21	0.21	6	1.000	45.00	1.329	0.583	0	0	0.055	0.033
DWPF PS 434	510	PS			0.222	0.197	2	1	43.59	1.368	0.537	0.015	0.007	0.088	0.033
DWPF PS 520	418	PS			0.231	0.16	2	1	46.65	1.422	0.624	0.006	0.007	0.127	0.033
DWPF MFT 558	418	MFT			0.474	0.22	2	0.886	41.62	0.741	0.255	0.006	0.007	0.095	0.115
DWPF MFT 558	418	MFT			0.41	0.212	2	0.693	41.62	0.843	0.338	0.006	0.007	0.095	0.234
DWPF MFT 568	418	MFT			0.157	0.06	3	0.464	39.88	0.671	0.309	0.006	0.007	0.135	0.327
DWPF MFT 568	418	MFT			0.057	0.029	3	0.517	39.88	0.671	0.309	0.006	0.007	0.135	0.327
DWPF MFT 568	418	MFT			0.025	0.012	3	0.383	39.88	0.742	0.346	0.006	0.007	0.135	
DWPF MFT 580	418	MFT			0.029	0.012	3	0.512	42.38	0.742	0.346	0.05	0.007	0.114	
DWPF MFT 580	418	MFT			0.04	0.023	3	0.483	42.38	0.742	0.346	0.05	0.007	0.114	
DWPF MFT 580	418	MFT			0.05	0.023	3	0.415	42.38	0.689	0.396	0.05	0.007	0.114	

Sample ID	Frit	SRAT/SME(MFT)	Target Waste Loading	SRAT pH	Measured REDOX	Fe^{+2} (units of absorbance)	# Fe Measurements	Total Fe (units of absorbance)	SME wt% solids	Formate (mol/kg)	Nitrate (mol/kg)	Oxalate (mol/kg)	Coal (mol/kg)	Mn (mol/kg)	Antifoam (mol/kg)
DWPF MFT 592	418	MFT			0.021	0.021	3	0.562	41.71	0.689	0.396	0.046	0.007	0.117	
DWPF MFT 592	418	MFT			0.022	0.022	3	0.462	41.71	0.689	0.396	0.046	0.007	0.117	
DWPF MFT 592	418	MFT			0.025	0.025	3	0.969	41.71	0.708	0.335	0.046	0.007	0.117	

APPENDIX C. Glycol REDOX Database for NG Flowsheet

Table C1. GLYCOL REDOX DATABASE (CC_{hot})*

Sample ID	Frit	SRAT/SME (MFT)	Target Waste Load	Fe^{2+} (units of absorbance)	# Fe Measurements	Total Fe (units of absorbance)	Formate (mol/kg)	Oxalate (mol/kg)	Coal (mol/kg)	Nitrate (+nitrite) (mol/kg)	Glycol Only (mol/kg)	Any Mn (mol/kg)	Anti-foam Carbon (mol/kg)
SB9-NG-51-7	418	SME	39	0.0535	6	0.497	0.015	0.101	0.00	0.708	0.47	0.2032	0.025
SB9-NG-51-8	418	SME	39	0.06	6	0.434	0.015	0.101	0.00	0.708	0.47	0.2032	0.025
SB9-NG-51-9	418	SME	39	0.053	6	0.41	0.015	0.101	0.00	0.708	0.47	0.2032	0.025
SB9-NG-52-7	418	SME	39	0.258	6	0.6055	0.013	0.066	0.00	0.722	0.685	0.165	0.031
SB9-NG-52-8	418	SME	39	0.2505	6	0.407	0.013	0.066	0.00	0.722	0.685	0.165	0.031
SB9-NG-52-9	418	SME	39	0.2185	6	0.493	0.013	0.066	0.00	0.722	0.685	0.165	0.031
SB9-NG-53-7	418	SME	39	0.2185	6	0.427	0.027	0.1	0.00	0.587	0.496	0.1961	0.025
SB9-NG-53-8	418	SME	39	0.21	6	0.44	0.027	0.1	0.00	0.587	0.496	0.1961	0.025
SB9-NG-53-9	418	SME	39	0.2735	6	0.452	0.027	0.1	0.00	0.587	0.496	0.1961	0.025
SB9-NG-54-7	418	SME	39	0.107	6	0.4395	0.00	0.062	0.00	0.869	0.585	0.184	0.035
SB9-NG-54-8	418	SME	39	0.112	6	0.551	0.00	0.062	0.00	0.869	0.585	0.184	0.035
SB9-NG-54-9	418	SME	39	0.0805	6	0.4535	0.00	0.062	0.00	0.869	0.585	0.184	0.035
SB9-NG-55-7	418	SME	39	0.1465	6	0.592	0.00	0.107	0.00	0.853	0.639	0.2183	0.028
SB9-NG-55-8	418	SME	39	0.1625	6	0.4195	0.00	0.107	0.00	0.853	0.639	0.2183	0.028
SB9-NG-55-9	418	SME	39	0.162	6	0.434	0.00	0.107	0.00	0.853	0.639	0.2183	0.028
SB9-NG-55A-10	418	SME	39	0.093	6	0.397	0.00	0.063	0.00	0.637	0.439	0.1375	0.01
SB9-NG-55A-11	418	SME	39	0.1255	6	0.401	0.00	0.063	0.00	0.637	0.439	0.1375	0.01
SB9-NG-55A-12	418	SME	39	0.1735	6	0.495	0.00	0.063	0.00	0.637	0.439	0.1375	0.01
SB9-NG-56-7	418	SME	39	0.051	6	0.419	0.00	0.095	0.00	0.862	0.52	0.1904	0.025
SB9-NG-56-8	418	SME	39	0.0375	6	0.407	0.00	0.095	0.00	0.862	0.52	0.1904	0.025
SB9-NG-56-9	418	SME	39	0.0625	6	0.589	0.00	0.095	0.00	0.862	0.52	0.1904	0.025
SB9-NG-57-7	418	SME	39	0.376	6	0.5335	0.00	0.095	0.00	0.717	0.736	0.1957	0.025
SB9-NG-57-8	418	SME	39	0.309	6	0.436	0.00	0.095	0.00	0.717	0.736	0.1957	0.025
SB9-NG-57-9	418	SME	39	0.3435	6	0.4695	0.00	0.095	0.00	0.717	0.736	0.1957	0.025
SB9-NG-58-7	418	SME	39	0.1155	6	0.42	0.021	0.113	0.00	0.629	0.487	0.2	0.015
SB9-NG-58-8	418	SME	39	0.1125	6	0.48	0.021	0.113	0.00	0.629	0.487	0.2	0.015
SB9-NG-58-9	418	SME	39	0.126	6	0.447	0.021	0.113	0.00	0.629	0.487	0.2	0.015
SB9-NG-59-13	418	SME	39	0.234	6	0.478	0.011	0.047	0.00	0.686	0.515	0.2285	0.023
SB9-NG-59-14	418	SME	39	0.244	6	0.547	0.011	0.047	0.00	0.686	0.515	0.2285	0.023
SB9-NG-59-15	418	SME	39	0.212	6	0.441	0.011	0.047	0.00	0.686	0.515	0.2285	0.023
SB9-NG-60-4	418	SME	39	0.0965	6	0.3505	0.00	0.086	0.00	0.885	0.582	0.2075	0.021

Sample ID	Frit	SRAT/SME (MFT)	Target Waste Load	Fe^{2+} (units of absorbance)	# Fe Measurements	Total Fe (units of absorbance)	Formate (mol/kg)	Oxalate (mol/kg)	Coal (mol/kg)	Nitrate (+nitrite) (mol/kg)	Glycol Only (mol/kg)	Any Mn (mol/kg)	Anti-foam Carbon (mol/kg)
SB9-NG-60-5	418	SME	39	0.077	6	0.4	0.00	0.086	0.00	0.885	0.582	0.2075	0.021
SB9-NG-60-6	418	SME	38	0.0895	6	0.3455	0.00	0.086	0.00	0.885	0.582	0.2075	0.021
SB9-NG-62-7	418	SME	38	0.13	6	0.4195	0.014	0.078	0.00	0.886	0.619	0.1982	0.028
SB9-NG-62-8	418	SME	38	0.1245	6	0.345	0.014	0.078	0.00	0.886	0.619	0.1982	0.028
SB9-NG-62-9	418	SME	38	0.1735	6	0.496	0.014	0.078	0.00	0.886	0.619	0.1982	0.028
SB9-BP1-1	418	SME	39	0.073	6	0.5045	0.012	0.093	0.00	0.738	0.491	0.1993	0.02688
SB9-BP1-2	418	SME	39	0.077	6	0.453	0.012	0.093	0.00	0.738	0.491	0.1993	0.02688
SB9-BP2-1	418	SME	39	0.0865	6	0.47	0.00	0.078	0.00	0.865	0.552	0.1872	0.03
SB9-BP2-2	418	SME	39	0.0965	6	0.491	0.00	0.078	0.00	0.865	0.552	0.1872	0.03
SB9-BP2-3	418	SME	39	0.1045	6	0.4375	0.00	0.078	0.00	0.865	0.552	0.1872	0.03
SB9-BP3-1	418	SME	39	0.0785	6	0.423	0.017	0.101	0.00	0.689	0.474	0.2021	0.025
SB9-BP3-2	418	SME	39	0.0905	6	0.4205	0.017	0.101	0.00	0.689	0.474	0.2021	0.025
SB9-BP3-3	418	SME	39	0.073	6	0.439	0.017	0.101	0.00	0.689	0.474	0.2021	0.025
SB9-BP4-1	418	SME	39	0.189	6	0.5435	0.009	0.099	0.00	0.711	0.568	0.2004	0.025
SB9-BP4-2	418	SME	39	0.149	6	0.46	0.009	0.099	0.00	0.711	0.568	0.2004	0.025
SB9-BP4-3	418	SME	39	0.2125	6	0.6015	0.009	0.099	0.00	0.711	0.568	0.2004	0.025

*Shaded rows are not used in REDOX modeling

References

1 H.D. Schreiber, and A.L. Hockman, **"Redox Chemistry in Candidate Glasses for Nuclear Waste Immobilization,"** Journal of the American Ceramic Society., V. 70[8], 591-594 (1987).

2 C.M. Jantzen and M.J. Plodinec, **"Composition and Redox Control of Waste Glasses: Recommendation for Process Control Limit,"** U.S. DOE Report DPST-86-00773, E.I. duPont deNemours & Co., Savannah River Laboratory, Aiken, SC (1986).

3 C.M. Jantzen, J.B. Pickett, K.G. Brown, T.B. Edwards, D.C. Beam, **"Process/Product Models for the Defense Waste Processing Facility (DWPF): Part I. Predicting Glass Durability from Composition Using a Thermodynamic Hydration Energy Reaction MOdel (THERMO™),"** U.S. DOE Report WSRC-TR-93-0672, Westinghouse Savannah River Co., Savannah River Technology Center, Aiken, SC, 464p. (1995).

4 C.M. Jantzen, K.J.Imrich, K.G. Brown, and J.B. Pickett, **"High Chrome Refractory Characterization: Part I. Impact of Melt REDuction/Oxidation (REDOX) on the Corrosion Mechanism in Radioactive Waste Glass Melters,"** International Journal of Applied Glass Science, 6[2], 137-157 (2015).

5 C.M. Jantzen, K.J.Imrich, K.G. Brown, and J.B. Pickett, **"High Chrome Refractory Characterization: Part II. Accumulation of Spinel Corrosion Deposits in Radioactive Waste Glass Melters,"** International Journal of Applied Glass Science, 6[2], 158-171 (2015).

6 M.E. Smith and D.C. Iverson, **"Installation of Bubblers in the Savannah River Site Defense Waste Processing Facility Melter,"** U.S. DOE Report SRR-STI-2010-00784, Savannah River Remediation, LLC, Aiken, SC (2010).

7 B.O. Mysen and P. Richet, **"Volatiles II. Noble Gases and Halogens,"** in **"Silicate Glasses and Melts,"** Elsevier Publishers, New York, New York pp.483-502 (2005).

8 G.I. Marziano, A. Paonita, A. Rizzo, B. Scaillet, and F. Gaillard, **"Noble Gas Solubilities in Silicate Melts: New Experimental Results and a Comprehensive Model of the Effects of Liquid Composition, Temperature and Pressure,"** Chemical Geology, 279 [3-4],145-157 (2010).

9 F.W. Kramer, **"Solubility of Gases in Glass Melts,"** in **"Properties of Glass-Forming Melts,"** L.D. Pye, A. Montenero, and I. Joseph (Eds.), CRC Press, Boca Raton FL, pp. 405-482 (2005).

10 D.M. Missimer, A.R. Jurgensen and R. Rutherford, **"High Temperature X-ray Diffraction Analyses of Simulated DWPF Sludge Batch 2 SRAT Products,"** U.S. DOE Memorandum SRNL-L4200-2009-00029, Savannah River Nuclear Solutions, Savannah River National Laboratory, Aiken, SC (2009).

11 D.M. Missimer, A.R. Jurgensen and R. Rutherford, "**High Temperature X-ray Diffraction Analyses of Simulated DWPF Sludge Batch 3 SRAT Products,"** U.S. DOE Memorandum SRNL-L4200-2009-00031, Savannah River Nuclear Solutions, Savannah River National Laboratory, Aiken, SC (2009).

12 D.M. Missimer, A.R. Jurgensen and R. Rutherford, **"High Temperature X-ray Diffraction Analyses of Simulated DWPF Sludge Batch 4 SRAT Products,"** U.S. DOE Memorandum SRNL-

L4200-2009-00033, Savannah River Nuclear Solutions, Savannah River National Laboratory, Aiken, SC(2009)

13 B.A. Hamm, R.E. Eibling, M.A. Ebra, T. Motyka, and H.D. Martin, **"High-Level Insoluble Waste Preparation for Vitrification,"** Scientific Basis for Nuclear Waste Management, VIII, C.M. Jantzen, M.A. Stone, and R.C. Ewing (Eds.), Materials Research Society, Pittsburgh, PA 793-799 (1985).

14 M.J. Plodinec, **"Foaming During Vitrification of SRP Waste,"** U.S. DOE Report DPST-86-213, E.I. duPont deNemours & Co., Savannah River Laboratory, Aiken, SC (1986).

15 W.G. Ramsey, C.M. Jantzen, and D.F. Bickford, **"Redox Analyses of SRS Melter Feed Slurry; Interactions Between Formate, Nitrate, and Phenol Based Dopants,"** Proceedings of the 5th Intl. Symposium on Ceramics in Nuclear Waste Management, G.G. Wicks, D.F. Bickford, and R. Bunnell (Eds.), American Ceramic Society, Westerville, OH, 259-266 (1991).

16 W.G. Ramsey, T.D. Taylor, K.M. Wiemers, C.M. Jantzen, N.D. Hutson, and D.F. Bickford, **"Effects of Formate and Nitrate Content on Savannah River and Hanford Waste Glass Redox"** Proceedings of the Advances in the Fusion and Processing of Glass, III, New Orleans, LA, D.F. Bickford, et.al. (Eds.) American Ceramic Society, Westerville, OH, 535-543 (1993).

17 W.G. Ramsey, N.M. Askew, and R.F. Schumacher, **"Prediction of Copper Precipitation in the DWPF Melter from the Melter Feed Formate and Nitrate Content,"** U.S. DOE Report WSRC-TR-92-385, Rev.0, Westinghouse Savannah River Co., Savannah River Technology Center, Aiken, SC (1994).

18 W.G. Ramsey, and R.F. Schumacher, **"Effects of Formate and Nitrate Concentration on Waste Glass Redox at High Copper Concentration,"** U.S. DOE Report, WSRC-TR-92-484, Rev. 0, Westinghouse Savannah River Co., Savannah River Technology Center, Aiken, SC (1992).

19 K.G. Brown, C.M. Jantzen, and J.B. Pickett, **"The Effects of Formate and Nitrate on REDuction/OXidation (REDOX) Process Control for the Defense Waste Processing Facility (DWPF),"** U.S. DOE Report WSRC-RP-97-34, Rev.0, Westinghouse Savannah River Co, Savannah River Technology Center, Aiken, SC (1997).

20 T.B. Calloway, C.M. Jantzen, L.M. Medich, and N.R. Spennato, **"Analysis of the DWPF Glass Pouring System Using Neural Networks,"** Waste Management '98 (1998).

21 M.J. Plodinec, **"Foaming and Dissolution of SRP Waste by Frit,"** U.S. DOE Report DPST-85-419, E.I. duPont deNemours & Co., Savannah River Laboratory, Aiken, SC (1985).

22 A.S. Choi, **"Validation of DWPF Melter Off-Gas Combustion Model,"** U.S. DOE Report WSRC-TR-2000-00100, Westinghouse Savannah River Co., Savannah River Technology Center, Aiken, SC (2000).

23 A.S. Choi, **"Prediction of Melter Off-Gas Explosiveness,"** U.S. DOE Report WSRC-TR-90-00346, Rev. 0, Westinghouse Savannah River Co., Savannah River Technology Center, Aiken, SC (, 1992).

24 C.M. Jantzen, J.R. Zamecnik, D.C. Koopman, C.C. Herman, and J.B. Pickett, **"Electron Equivalents Model for Controlling REDuction/OXidation (REDOX) Equilibrium During High Level Waste (HLW) Vitrification,"** U.S. DOE Report WSRC-TR-2003-00126, Rev.0, Westinghouse Savannah River Co., Savannah River Technology Center, Aiken, SC (2003).

25 C.M. Jantzen, D.C. Koopman, C.C. Herman, J.B. Pickett, and J.R. Zamecnik, **"Electron Equivalents REDOX Model for High Level Waste Vitrification,"** Environmental Issues and Waste Management Technologies IX, J.D. Vienna and D.R. Spearing (Eds), Ceramic Transactions 155, 79-91 (2004).

26 D.C. Koopman, C.C. Herman, and N.E. Bibler, **"Sludge Batch 3 Preliminary Acid Requirements Studies with Tank 8 Simulant,**" U.S. DOE Report WSRC-TR-2003-00041, Rev. 0, Westinghouse Savannah River Co., Savannah River Technology Center, Aiken, SC (2003).

27 D.C. Koopman, C.C. Herman, J.M. Pareizs, C.J. Bannochie, D.R. Best, N.E.Bibler, and T.L. Fellinger, **"Spontaneous Catalytic Wet Air Oxidation during Pretreatment of High-Level Radioactive Waste Sludge,"** SRNL-STI-2009-00611, International Atomic Energy Agency-International Nuclear Information System (IAEA-INIS) Volume 41[3] Ref.# 41010463 (2009).

28 D.C. Koopman, D.R. Best, and B.R. Pickenheim, **"SRAT Chemistry and Acid Consumption During Simulated DWPF Melter Preparation,"** U.S. DOE Report WSRC-STI-2008-00131, Rev. 0, Westinghouse Savannah River Co., Savannah River Technology Center, Aiken, SC (2008).

29 B.M. Rapko, G.J. Lumetta, **"Status Report on Phase Identification in Hanford Tank Sludges,**" U.S. DOE Report PNNL-13394, Battelle Memorial Institute, Pacific Northwest National Laboratory, Richland, WA (2000).

30 C.M. Jantzen and M.E. Stone, **"Role of Manganese Reduction/Oxidation (REDOX) on Foaming and Melt Rate in High Level Waste (HLW) Melters,"** U.S. DOE Report WSRC-STI-2006-00066, Rev.0, Westinghouse Savannah River Co., Savannah River Technology Center, Aiken, SC (2007).

31 C.M. Jantzen and F.C. Johnson, **"Impacts of Antifoam Additions and Argon Bubbling on Defense Waste Processing Facility (DWPF) REDuction/OXidation (REDOX),"** U.S. DOE Report SRNL-STI-2011-00652, Rev. 0, Westinghouse Savannah River Co., Savannah River Technology Center, Aiken, SC (2012).

32 A.S. Choi, **"DWPF Melter Off-Gas Flammability Assessment,"** Calculation Sheet X-CLC-S-00164, Rev. 8, Savannah River Nuclear Solutions, Savannah River National Laboraotory, Aiken, SC (2013).

33 D.P. Lambert, J.R. Zamecnik, J.D. Newell, and M.S. Williams, **"Antifoam Degradation Testing,"** U.S. DOE Report SRNL-STI-2015-00352, Rev. 0, Savannah River Nuclear Solutions, Savannah River National Laboratory, Aiken, SC (2015).

34 D.P. Lambert, D.C. Koopman, J.D. Newell, D.T. Wasan, A.P. Nikolov, E.K. Weinheimer, **"Improved Antifoam Agent Study-End of Year Report, EM Project 3.2.3,"** SRNL-STI-2011-00515, Rev. 0, Savannah River Nuclear Solutions, Savannah River National Laboratory, Aiken, SC (2011).

35 T.L. White, D.P. Lambert, J.R. Zamecnik, and W.T. Riley, **"Ion Chromatography (IC) Analyses of Glycolate in Simulated Waste,"** U.S. DOE Report, SRNL-STI-2015-00049, Rev. 0, Savannah River Nuclear Solutions, Savannah River National Laboratory, Aiken, SC (2015).

36 C.M. Jantzen, M.S. Williams, J.R. Zamecnik and D.M. Missimer, **"Interim Glycol Flowsheet REDuction/OXidation (REDOX) Model for the Defense Waste Processing Facility (DWPF),"**

U.S. DOE Report, SRNL-STI-2015-00702, Rev. 0, Savannah River Nuclear Solutions, Savannah River National Laboratory, Aiken, SC (2016).

37 C.M. Jantzen and T.B. Edwards, **"Defense Waste Processing Facility (DWPF) Viscosity Model: Revisions for Processing High TiO_2 Containing Glasses,"** U.S. DOE Report SRNL-STI-2016-00115, Rev.0, Savannah River Nuclear Solutions, Savannah River National Laboratory, Aiken, SC (2016).

38 C.J. Martino, **"Analysis of Precipitated White Solids from Nitric-Glycolic Flowsheet Chemical Processing Cell Products,"** Savannah River National Laboratory Memorandum SRNL-L3100-2016-00004, Rev. 0 (2016).

39 D.M. Missimer and R. Rutherford, **"High Temperature X-ray Diffraction (HTXRD) Analyses on the Glycol Flowsheet,"** Savannah River National Laboratory Memorandum SRNL-L4110-2015-00007, Rev. 0 (2015).

40 D.M. Missimer, A.R. Jurgensen and R. Rutherford, "**X-ray Diffraction Analyses of Heat Treated Simulated DWPF Sludge Batch 3 and 4 SME Feeds,"** Savannah River National Laboratory Memorandum SRNL-L4200-2009-00032, Rev. 0 (2009).

41 D.M. Missimer and R. Rutherford, **"X-ray Diffraction (XRD) Analyses on the Formic/Nitric, Glycolic/Nitric (GN) and Glycolic/Formic (GF) Flowsheet Samples,"** U.S. DOE Memorandum SRNL-L4110-2016-00003, Rev. 0, Savannah River Nuclear Solutions, Savannah River National Laboratory, Aiken, SC (2016).

42 C.W. Hsu, **"Defense Waste Processing Facility Nitric Acid Requirement for Treating Sludge,"** U.S. DOE Report WSRC-RP-92-1056, Westinghouse Savannah River Co., Savannah River Technology Center, Westinghouse Savannah River Co., Aiken, SC (1992).

43 D. P. Lambert, M. S. Williams, C. H. Brandenburg, M. C. Luther, J. D. Newell and W. H. Woodham, **"Sludge Batch 9 Simulant Runs Using the Nitric-Glycolic Acid Flowsheet,"** U.S. DOE Report SRNL-STI-2016-00319, Rev. 0, Savannah River Nuclear Solutions, Savannah River National Laboratory, Aiken, SC (2016).

44 **"Heat Treatment of Waste Slurries for REDOX And Corrosion Analyses,"** Procedure Manual L29, Procedure ITS-0052, Rev. 5, Savannah River Nuclear Solutions, Savannah River National Laboratory, Aiken, SC (2016).

45 E.W. Baumann, **"Colorimetric Determination of Iron (II) and Iron (III) in Glass,**" Analyst, 117, 913-916 (1992).

46 **"Determining Fe^{2+}/Fe^{3+} and Fe^{2+}/Fe (total) Using UV Vis Spectrometer,"** Procedure Manual L29, Procedure ITS-0042, Rev.2, Savannah River Nuclear Solutions, Savannah River National Laboratory, Aiken, SC (2014).

47 D.P. Lambert, **"Task Technical and Quality Assurance Plan for Phase II CPC Testing for Nitric-Glycolic Flowsheet Development,"** U.S. DOE Report SRNL-RP-2012-00762, Rev. 0, Savannah River Nuclear Solutions, Savannah River National Laboratory, Aiken, SC (2012).

48 T.L. Fellinger, "**Phase II – Nitric-Glycolic Acid Flowsheet Testing,**" HLW-DWPF-TTR-2013-0003, Rev. 0, Savannah River Remediation, Aiken, SC (2012).

49 E.W. Holtzscheiter, **"Bounding Alternate Reductant Testing/Chemistry and REDOX Definition,"** X-TTR-S-00024, Rev. 0, Savannah River Remediation, Aiken, SC (2014).

50 Basic Data Report for DWPF Sludge Plant, U.S. DOE Report DPST-80-1033, Rev. 91, E.I, DuPont deNemours & Co., Savannah River Site, Aiken, SC (1984).